Title:

Innovative Methods to Achieve Ultra-Low Coke Rate for Carbon-Neutral Blast Furnaces

Authors:

Takeshi Sekiguchi

Affiliations:

SimpLE-labo Co., Ltd., Yokohama, Japan

Corresponding author:

Takeshi Sekiguchi

email: sekiguchi@simple-labo.co.jp

Abstract:

The blast furnace (BF) remains the most energy-efficient ironmaking route worldwide, yet achieving deep decarbonization without compromising thermal efficiency is a critical challenge. This study proposes "SimpLE" (Smart Ironmaking Process for Low Emissions), an ultra-low coke rate (CR ≈ 60 kg/thm) concept that redefines the BF from a conventional reduction-gasifier to a high-efficiency melter coupled with a full-gas-based reduction shaft. This paradigm shift is achieved by integrating three innovations: Smart Reduction (confining reduction to the shaft for 100% gas-based reduction), Smart Charging (maintaining permeability via the coke-slit-less cohesive zone), and Smart Combustion (enabling nearly complete pulverized coal combustion without raceways). SimpLE BF thermodynamically transforms a "black-box-like 3-dimensional" mixed-reduction process into a "quasi-one-dimensional" gas-based reduction process, enabling the manipulation of critical variables such as reduction temperature. Accordingly, thermodynamic analysis, validated against industrial data, demonstrates that SimpLE reduces fossil-derived input carbon by ~38–41% (or ~53% with green-H_2), with total CO_2 reduction reaching ~60–68% via carbon recycling. Also, the pressure-drop head is estimated to be ~1/10 in the cohesive zone and decreases to ~43–60% in total compared to conventional BFs. This work validates the process-level feasibility of the concept and provides a scientific basis for future pilot-

plant verification. Ultra-low CR BF will be a robust platform for carbon neutralization, replacing fossil fuels with circular resources such as waste materials.

Keywords:

blast furnace; carbon neutral; coke rate; raceway; smart combustion; smart reduction

1. Introduction

Blast furnaces (hereafter BF) have long played a central role in steel production because of their superior productivity and excellent thermal efficiency. However, the global shift toward a carbon-neutral (CN) society has heightened concerns over CO_2 emissions, prompting numerous projects to reduce BF emissions [1-3]. For instance, the ULCOS-BF in Europe [4,5] aimed to reduce input carbon (hereafter Input C) by over 20% and total CO_2 by 50% using CO_2 capture, utilization, and storage (CCUS). However, the project was discontinued before plant verification due to the rapid shift toward carbon neutrality. Similarly, Japan's COURSE50 [2,6] targets only a 10% reduction in Input C, with a total CO_2 reduction of 30% including CCUS.

Meanwhile, development is underway on hydrogen-based reduction technologies[2] to replace the blast furnace process. However, hydrogen production and transportation are energy- and cost-intensive, and constraints in energy supply and infrastructure have hindered widespread adoption. Furthermore, the combined process of hydrogen-based direct reduced iron (DRI) and electric melting (hereafter, H_2-DRI+Melter) faces several technical challenges, including DRI quality control, CO_2 emissions from electricity, and issues inherent in hydrogen reduction, such as low gas utilization efficiency.

The BF is a highly thermally efficient process that enables continuous production of hot metal from iron ore. If fuel and reducing agents such as coke and pulverized coal (hereafter PC) are minimized and replaced with low-carbon sources such as municipal solid waste (MSW)[7] toward carbon-neutrality (CN), it offers the potential for greater thermal and economic efficiency than alternative processes. However, a large amount of coke is considered indispensable in the conventional BFs and the reduction of coke rate (hereafter CR: the amount of coke per 1 ton of hot metal) is subject to major limiting factors: (1) a thermodynamic limit as a heat source required to maintain heat and mass balance, (2) thermodynamic and kinetic limits coming from combustibility competition with PC as a coke substitute, and (3) a lower limit as structural support and ventilation material for furnace permeability. Furthermore, CR has another limit (4) of economy. Since the supply of coal-derived gases such as coke oven gas (COG) and BF gas (BFG) has

been economical for steelworks as a whole, little research has focused on drastically reducing the CR. Historically, the lower limit of CR has been considered to be around 200-250 kg/thm[2,3, 8-10].

To address these challenges, this study proposes an innovative BF process—"SimpLE" (Smart iron-making process for Low Emissions)[11]—redefined to enable ultra-low CR operation based on four key perspectives:

i) **Thermodynamics**: Converting direct reduction—consuming coke and much heat— into gas-based reduction by injecting sufficient reducing gas, which can be derived not only from BF top gas—like ULCOS BF— but also from external reforming-fuels such as COG or natural gas (shown as NG or CH_4 in figures).

ii) **PC Combustion Design:** Achieving highly preferential PC combustion over coke to get high PC combustion efficiency and ultra-low CR operation together.

iii) **Furnace Permeability:** Improving the permeability even in ultra-low CR operation through burden-charging control and gas-flow control.

iv) **Input C:** Shifting the positive evaluation of a BF as a coal gasifier to minimizing heat consumption and input C for ironmaking, shifting the fuel from coal—especially coking coal—to internal surplus energy and low-carbon fuels such as natural gas (hereafter NG; shown as CH_4 in figures) or MSW (in future)[7].

In particular, this study identifies the maximization of PC combustion efficiency under ultra-low CR operation as a key technical challenge as follows.

In the small-scale experimental furnace of the ULCOS BF, a PC rate (hereafter PCR) of 170kg/thm, a CR of 230kg/thm were achieved[4]. However, the experimental PC combustion efficiency (for high-volatile coal) was reported to be ≤50%[5], suggesting that over 85 kg/thm of unburnt PC (UPC) may have been generated. Unburnt PC is considered to be consumed in the conventional BF as direct reduction ($FeO+C = Fe+CO$) or gasification ($C+CO_2 = 2CO$)—the latter is equivalent to direct reduction coupled with gas-based reduction ($FeO+CO = Fe+CO_2$). However, since the direct reduction degree (hereafter DRR) of ULCOS was 5 to 15%[4], it seemed that the operation far-exceeded the potential limit of consumption via direct reduction (30 kgC/thm when DRR=10%). Therefore, it

requires additional consumption via carburization, which also appeared to have nearly reached the potential limit (Fig. 1).

Since SimpLE BF pursues complete gas-based reduction—DRR=0%, unburnt PC is not expected to be consumed via direct reduction. Drastic concept change was needed to achieve higher PCR and lower CR as shown in Fig. 1.

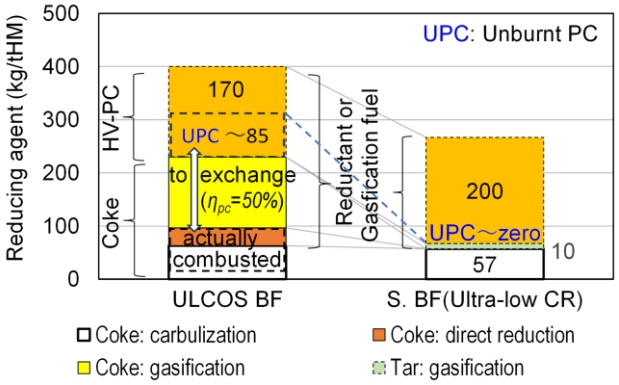

Fig. 1. Minimization of coke and unburnt PC (Image)

Conventionally, it has been considered essential to use high-volatile (HV) coals with high ignitability and combustibility, along with a deep raceway (RW) formed by hot blast through the tuyere, as the PC combustion zone [5,13-18]. However, the raceway primarily serves to crush and combust strong lump coke, which inevitably generates a large amount of coke dust (CKD) [19,20]. Since coke combusts more easily as its particle size decreases [14], this can lead to a decline in PC combustion efficiency.

This study aims to maximize PC combustion efficiency under ultra-low CR conditions. We propose a strategy to reduce blast velocity, thereby eliminating the raceway and deadman. This “raceway-free” approach stabilizes the coke bed near the tuyere, suppressing coke fragmentation and promoting PC preferential combustion.

In addition, to address concerns about the deterioration of furnace permeability associated with the ultra-low CR, it was confirmed that permeability can be significantly improved by suppressing coke dust accumulation in the dripping zone and coke bed through innovations in charging method and enhancement of gas reduction.

[Structure of the Study] This study focuses on the technical feasibility and potential impacts of SimpLE BF compared to conventional BFs, across four areas:

i) **Process Concepts** (Section 2),

ii) **Heat and Mass Balance and CO_2 reduction potential** (Section 3),

iii) **PC Combustion/Consumption Dynamics** (Sections 4.1–4.2), and

iv) **Furnace Permeability** (Sections 4.3–4.4).

To ensure reliability, we employ a **rigorous dual-approach**: Theoretical concepts/models are deductively derived and then inductively validated against conventional-BF baselines and diverse industrial datasets. For ii) and iv), we apply direct validation using empirically validated engineering models and operational/literature data. However, for iii) (PC combustion) where direct data for raceway-free combustion is limited, we deductively construct a **widely applicable estimation tool** that is verified to unify disparate and diverse & seemingly-inconsistent industrial datasets like a Rosetta Stone, verifying **t**he new concept. **[Future Scope]** Plant-level engineering and industrial trials toward a reference plant will be addressed in future phases. This study establishes the theoretical foundation of ultra-low CR BFs (Step 1), while Step 2 [7] utilizes waste-derived fuels including MSW to enable near-zero fossil carbon input and negative emissions.

2. Concept of Ultra-Low CR BF and Associated Process Innovations

2.1 Overall Concept and Core Philosophy

SimpLE Innovation: SimpLE BF targets near-zero emissions and ultra-low coke rate (CR). It innovates three core functions—charging, reduction, and combustion—to comprehensively address the BF's essential challenges: efficiently supplying reducing gas and heat to the ore reduction zone while maintaining the permeability.

Three Synergistic Concepts:

i) **Smart Reduction:** Targets 100% gas reduction by concentrating the reduction in the shaft under controlled temperatures, thereby preventing low-temperature ore disintegration at and high-temperature coke degradation. Top gas recycling (hereafter TGR) is essential; fully reusing top gas (in-furnace or as hot-stove fuel) eliminates surplus gas discharge. This boosts gas utilization to nearly 100% and significantly lowers Input C and CO_2. The system is thermodynamically viable and ensures sufficient permeability, offering a novel operation theory beyond the traditional black-box model.

ii) Smart Charging: Ensures high permeability in both the cohesive zone and shaft under ultra-low CR operation. It also optimizes shaft gas distribution via burden control.

iii) Smart Combustion: Enhances PC combustion by reducing blast velocity to eliminate the raceway. This suppresses coke fragmentation and prevents dust generation, which improves gas flow and permeability in the lower furnace (from cohesive zone to hearth).

2.2 Characteristics and Configuration of SimpLE BF

Route Comparison (Fig. 2): Fig. 2 (adapted from Ref [7]) compares the conventional BF, SimpLE BF, and a DRI+Melter system. In the DRI+Melter process, hot metal is produced by high-ratio gas-based reduction (~96%) using reformed gas from CH_4 or external H_2—a mechanism thermodynamically similar to Smart Reduction—followed by electric melting. However, the DRI+Melter process itself faces logistical and operational challenges,

including: handling/distribution of high-temperature DRI, melting/carburization efficiency, productivity, refractory lifespan, exhaust gas treatment, and slag management.

Furthermore, H_2 route (H_2-DRI+Melter) faces multiple challenges such as low thermal efficiency, economic viability, H_2 availability, and high-temperature large electric heaters.

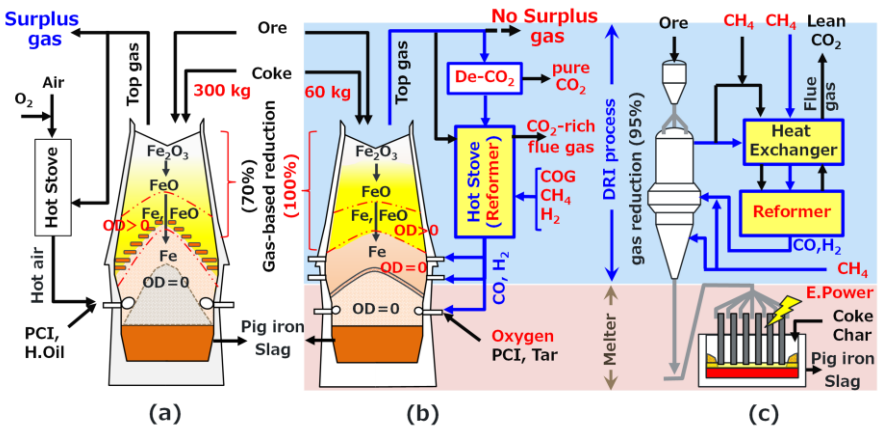

Figure 2. Schematic comparison of ironmaking routes: (a) conventional BF; (b) SimpLE BF; (c) DRI + melter.

Integrated Process: In contrast, SimpLE BF maintains the continuous flow of a conventional BF. Because "Smart Reduction" enables gas-based reduction by nearly 100% instead of 70% for conventional BF, the lower furnace effectively functions as a melter. Consequently, SimpLE BF uniquely integrates DRI process and Melter function within a unified thermodynamic and logistical system.

System Configuration: SimpLE BF features:

i) **Smart Reduction:** TGR with CO_2 separator (hereafter De-CO_2), fuel gas reformer, and a three-stage tuyere system.

ii) **Smart Charging:** Full-mixed charging and a coke-slit-less cohesive zone.

iii) **Smart Combustion:** Mild-blast tuyeres and a coke bed without raceway or deadman.

2.3 Process Innovation for Ultra-Low CR

(1) Innovations in Cohesive Zone Structure and Charging Control

At ultra-low CR, the coke slits in the cohesive zone become too thin to maintain permeability. Since mixing coke into ore is known to enhance cohesive layer permeability [21,22], Smart Charging adopts full mixing of coke and ore. Ultra-low CR is too small to form slits but enough to form a coke-slit-less cohesive zone with enhanced permeability, which is also within the well-industrialized mixing range[21]. Furthermore, approaching

100% gas-based reduction raises the ore's softening/melting points, suppressing FeO melt formation and further improving permeability [23–25]. Additionally, alternating layers of large (O_L) and small (O_S) ore optimize stable gas flow and improve the permeability in the shaft.

(2) Shafts (Innovation in the Reduction Process)

Comparison of Shaft Systems (Fig. 3): Fig. 3 compares the shaft injection concepts: (a) conventional shaft-injection, (b) Smart Reduction (three-stage tuyeres), and (c) DRI shaft furnace. (a) Conventional shaft-injection suffers from reduction deficiency in the central—physically inevitable due to poor gas penetration[2,9,26]. (c) DRI shaft furnaces face internal cooling-gas leakage that produces a central heat deficit, decreasing the central reduction degree [27]—inherently unavoidable for DRI to be cooled and supplied to an external melter. In contrast, (b) Smart Reduction (SimpLE BF) realizes a thermodynamically 100% gas-based reducing environment by means of a three-stage tuyere system coupled with an internal melter—creating a quasi-one-dimensional thermodynamic homogeneity without penetration issue or cooling gas issue.

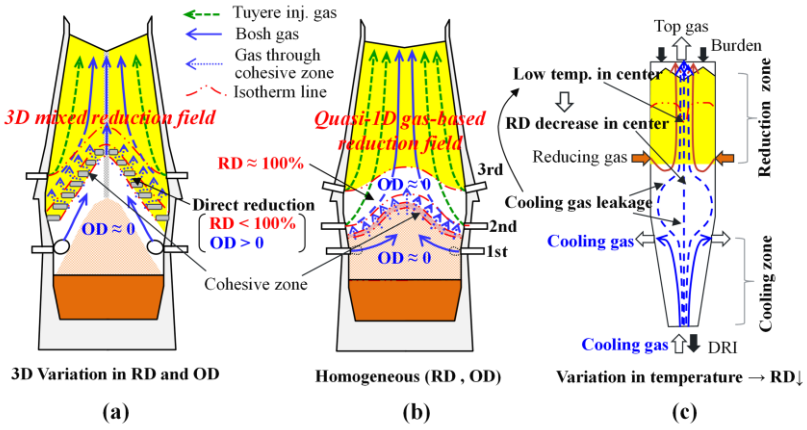

Figure 3. Schematic comparison of shaft-injection systems: (a) Conventional shaft-injection; (b) Smart Reduction (three-stage tuyeres); (c) DRI shaft furnace

Gas Flows and Isotherms: The top gas after CO_2 removal and the reformed gas are injected through a three-stage tuyere system (Fig. 3(b)). Aside from penetration issues, combustion gas (bosh gas) from the first-stage tuyeres flows through the furnace center, while gases from the second- and third-stage tuyeres flow toward the intermediate and wall regions. On the other hand, in blast furnaces, gas and material flows form isotherms, where the cohesive zone is physically formed along the isotherms (Figs. 3(a), 3(b)) and the injection-gas temperatures act as the rooting points. In SimpLE, the cohesive zone

temperature is approximately 1350℃ ~ 1450℃, therefore the zone is thermodynamically held stably below the second-stage tuyere (≈1300℃) and above the first-stage tuyere (≥2000℃). By eliminating coke slits and reducing the bosh gas rate, the isotherms of SimpLE's cohesive zone become much more gradual than the steep inverse-V shape of conventional BFs'.

Quasi-one-dimensional Thermodynamic Homogeneity: In SimpLE BF, the reducing-gas flow rate is adjusted by the recycling top gas and reformer fuels (COG, natural gas, etc.) so that the ore's reduction degree (RD) approaches 100% at the shaft bottom, thermodynamically anchoring the Rist operating line at (x, y) ≈ (1, 0). Meanwhile, all tuyeres supply reducing gas with an oxidation degree (OD) ≈ 0—x ≈ 1 in the Rist diagram. Also, the bosh (OD ≈ 0) gas from the first-stage tuyeres passes through the FeO-free cohesive zone at OD ≈ 0. Consequently, all the gas and ore at the shaft bottom is thermodynamically homogeneous (OD ≈ 0, RD ≈ 100%) across the furnace (Fig. 3(b)), even without hydrodynamic gas-mixing. This forms a quasi-one-dimensional counter-current gas-reduction field in the shaft, which practically harmonizes with one-dimensional analysis such as heat/mass balance and equilibrium reaction models including the Rist diagram. This is significantly different from conventional BFs which have 3-dimensional OD and RD distributions in the shaft and cohesive zone, requiring 3-dimensional analysis and complicated calibration. These differences determine the controllability of the process as well.

Process Controllability: By regulating gas flows through the three-stage tuyeres, the quasi-one-dimensional gas-reduction field can be controlled, thereby improving reaction efficiency and suppressing low-temperature disintegration of ore and preventing coke gasification—core objectives of Smart Reduction. Also, adjusting the flow-rate split between the first- and second-stage tuyeres without changing the summation controls lower-furnace heat parameters independently of shaft reduction conditions.

Thermal Profile (vs. Conventional BF): Figs. 4 and 5[7] show the one-dimensional heat transfer diagrams analyzed between burden and gas. In the conventional BF, the temperature at point W (thermal reserve zone) reaches ~950 °C, and ore reduction—with sub-generation of CO_2 /H_2—continues until melting in the lower furnace. Consequently, the gasification of coke by CO_2 /H_2 is inevitable. Further, the gas flows 3-dimensionally in reality due to raceways and coke slits, making OD/RD distributions and the temperature profile complex and difficult to control (Fig. 3(a)). In contrast, SimpLE BF forms a quasi-one-dimensional gas-based reduction field (Fig. 3(b)). The start and end temperatures of ore reduction can be selectively controlled via the three-stage tuyere system (Fig. 5), with the point W temperature consequently adjusted in between. This allows full reduction, for example, within the 600–900 °C range, thereby suppressing low-temperature disintegration of ore and preventing coke gasification. A 100% gas-based reduction ratio is also thermodynamically feasible under such controlled conditions.

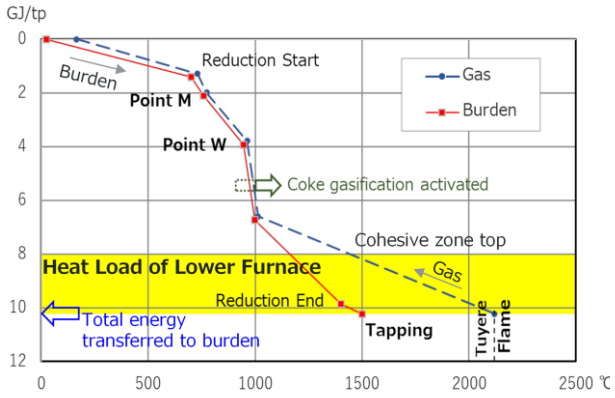

Figure 4. Heat transfer diagram of Conventional BF (Calculation results of Conv.BF in Table 3)

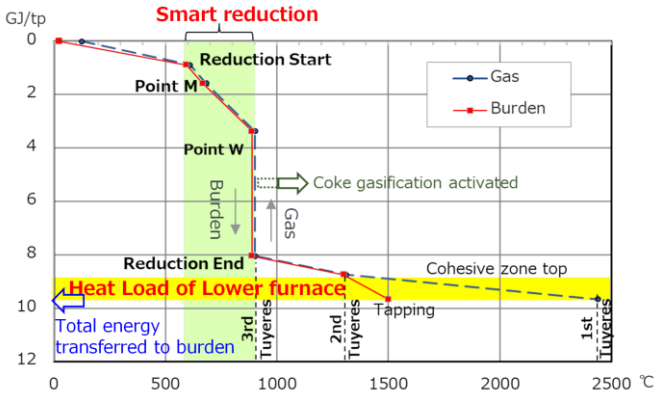

Figure 5. Heat transfer diagram of SimpLE BF (Calculation results of S.BF-1 in Table 3)

Unlocking the Black Box: This configuration enables, from a thermodynamic point of view, quasi-independent control of the melting zone (lower furnace) and the gas-reduction zone (shaft). Combined with the realization of a quasi-one-dimensional reaction field, Smart Reduction successfully transforms the **black-box-like** blast furnace into a process that is thermodynamically easier to adjust and control.

Kinetic Validity (Deductive approach): In addition to thermodynamic feasibility, the kinetic validity of SimpLE BF has been deductively confirmed from reaction rate and heat

transfer rate viewpoints.

- **Reduction Reaction Rate:** N_2 and H_2 in a conventional BF are substituted for $CO+H_2$ mixed gas reformed from COG and natural gas, while keeping the same CO partial pressure as in the conventional BF. H_2 reduces iron ore faster than CO and does not primarily compete with it in the reduction reactions [28], which is consistent with the Rist diagram methodology for $CO+H_2$ mixed gas. Therefore, the gas-based reduction ratio increases to close to 100% (approx. 70% by CO, 30% by H_2) for the same reaction time as the conventional BF's.
- **Reaction Time vs. Retention Time:** Lowering the gas-based reduction temperature from 1000 °C to 900 °C to suppress coke gasification may decrease the wustite reduction rate by approx. 25% [29,30]. However, under ultra-low CR operation, the ore-to-coke ratio (O/C) increases, extending the ore retention time in the shaft by about **80%—** when CR is reduced from 300 to 60 kg/thm; sinter ratio=0.85; bulk densities(t/m^3) =1.8(sinter), 2.5(lumpy ore), and 0.45(coke). Thereby, sufficient reduction time is ensured.
- **Heat Transfer Rate:** As shown in the heat transfer diagrams (Figs. 4 and 5), the total heat transferred in the shaft (above the cohesive zone) is lower in SimpLE BF (8.8 GJ/thm) than in the conventional BF (9.5 GJ/thm), confirming feasibility from a heat transfer viewpoint for the same productivity.

Kinetic Validity (Inductive approach): We further validated this inductively against the ULCOS BF's experimental result. The productivity was 4.4 $t/m^3 \cdot day$ [2,4]—double that of a conventional BF—with a direct reduction ratio (DRR) of ≈6% under a shaft-injection rate of ≈670Nm^3/thm ($CO+H_2$). It was implied that DRR could be lower with more gas injection [4]. Therefore, kinetic speed will not be an issue in SimpLE BF at least for the conventional productivity. Further, it verifies the possibility of the same productivity (4.4 $t/m^3 \cdot day$) for SimpLE BF considering the external-fuel reforming system and the quasi-one-dimensional reduction field.

(3) Lower Furnace: Innovations in Thermal Load, Combustion, and Permeability

1) Thermal Load Reduction in the Lower Furnace via Elimination of Direct Reduction

The fully reduced, high-temperature metallic iron is melted by the combustion of fuel and oxygen injected through the first-stage tuyeres (conventional tuyere level). Absence of direct reduction in the lower furnace reduces the thermal load to one-third of that in a conventional BF (see Fig. 5). Consequently, both the fuel rate and the volume of bosh gas can be reduced to one-half to one-third of conventional levels (see Table 3).

2) Fuel Selection and Pre-treatment: External Management of Endothermic Decomposition

To minimize cooling caused by endothermic decomposition, COG and natural gas are reformed, and high-volatile coal is subjected to carbonization prior to use. Similarly, for flame temperature control at the tuyere tip, preheated reducing gases (CO and H_2) are used in place of substances such as H_2O, CO_2, and CH_4, which clearly impose a cooling load through decomposition.

3) Enhanced PC Combustion and Suppression of Coke Pulverization through Raceway Elimination

The lower furnace is filled with high-strength, large-size, and low-reactivity coke with no prior gasification history (hereafter, strong lump coke). Although the conventional PC combustion zone is narrowed due to the elimination of the raceway by reducing blast velocity, PC still combusts preferentially over strong lump coke even within the coke-packed bed. This behavior was quantitatively validated in Section 4 in terms of PC combustion efficiency, demonstrating that even under ultra-low CR conditions—with high PC/O_2 ratios (oxygen excess ratio < 1)—high combustion efficiency can be achieved (Smart Combustion concept).

4) Coke-slit-less Cohesive Zone

In SimpLE BF, the cohesive zone and the cohesive layer become effectively unified due to the absence of coke slits—a structure formed by full-mixed charging. Consequently, all ascending gas must pass through the cohesive layer, enhancing heat exchange efficiency and leading to a thinner cohesive zone. Furthermore, the combination of full-mixed charging and 100% gas-based reduction improves the gas permeability of the cohesive layer itself, significantly reducing pressure drop. Additionally, coke fines and

unburnt PC generated in the lower furnace cannot pass through the cohesive layer and are thus re-consumed in the lower furnace, causing the apparent PC combustion efficiency to asymptotically approach 100%.

5) Improvement of Lower Furnace Permeability

In conventional BFs, the surface strength of lump coke decreases to approximately one-third of its initial value due to gasification reactions[31]. Consequently, coke tends to undergo pulverization in the dripping zone—where shearing forces are generated by burden weight and constricted coke flow—and in the raceway—where it is subject to impact crushing by hot blast. This leads to coke fines accumulation on the surface and within the deadman, thereby obstructing both gas and liquid permeability[10,31].

In SimpLE BF, (1) degradation of coke is suppressed by Smart Reduction, (2) fragmentation and pulverization of coke is prevented by raceway elimination, and (3) deposition of coke fines is avoided by the absence of deadman. Accordingly, the gas and liquid permeability is substantially improved in the lower furnace, filled with strong lump coke.

6) Centralization of Bosh Gas Flow

In the lower furnace, gases are directed toward the shaft center by the effect of the three-stage tuyeres. Meanwhile, gas dispersion caused by pressure drops in the cohesive and lump zones moderates this flow, resulting in a gentle central stream (Fig. 3). Outside the vicinity of the tuyeres, the bosh gas reaches an oxidation degree of $OD = 0$, so no gasification or direct reduction occurs, allowing hot gas to reach the furnace center more easily.

3. Heat and Mass Balance, Heat Consumption and CO_2 Reduction Potential

3.1 Heat and Mass Balance

(1) Calculation Method

Calculation Model (Fig. 6): Supposing SimpLE BF is operated in practice under quasi-one-dimensional thermodynamics, the heat and mass balance calculations have been carried out using a one-dimensional blast-furnace model (Fig. 6). In this paper, unless otherwise noted, temperatures are expressed in °C, and pressures are given in absolute units (MPa). The temperature symbol T in equations represents the absolute temperature in K.

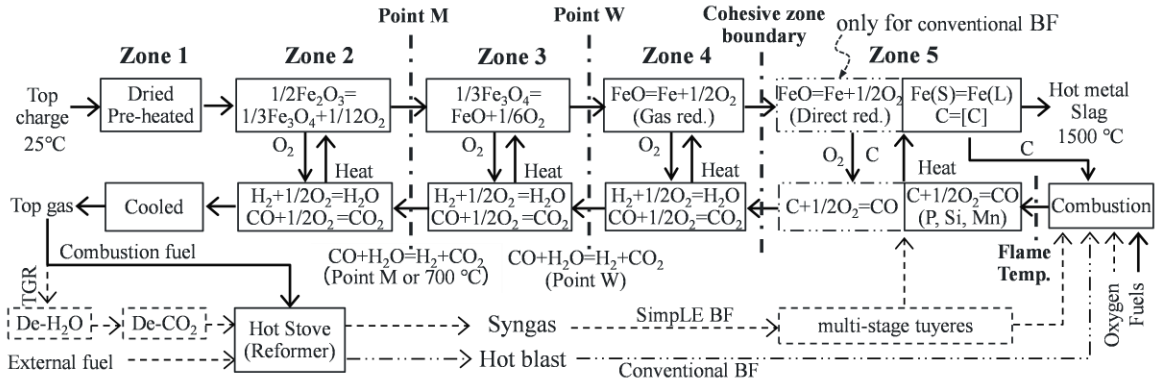

NOTE 1. Top charged carbon is assumed to be preheated up to Zone 5, where it is combusted or dissolved into hot metal.
2. Si, P, Mn is assumed to be produced in Zone 5 by direct reduction.
3. Point W, M temperatures are decided by heat balance, although which affects boundary conditions as well.

Figure 6. Heat mass balance calculation of BF

Calculation Procedure: The furnace is divided into five zones (Zone 1–5) and a thermodynamic balance is taken for each zone. The calculation proceeds as follows:

1. Top gas is first used for the hot stove (H/S) fuel ; the remainder is dried (De-H_2O), decarbonated (De-CO_2) and recycled as TGR gas.
2. TGR gas is preheated and reformed together with the external fuel (Fig. 6) whose amount is determined supplementarily from the heat and mass balance.
3. Gas supply conditions for the three-stage tuyeres are set as boundary conditions for Zone 5, based on tuyere-tip combustion calculations.
4. Assuming fuel rates, TGR ratio, and distributions/temperatures of tuyere-gases, a comprehensive heat and mass balance is calculated including the H/S.
5. Steps 1–4 are iterated; shaft efficiency and heat/mass balance errors are checked on the Rist diagram, and the operating parameters are adjusted until convergence.

Uniqueness of the Solution: For SimpLE BF, which operates with 0% direct reduction, a unique thermodynamic solution can be determined on the Rist diagram by specifying raw material conditions and two process variables (e.g., shaft efficiency and top gas

temperature). For conventional BFs, additional process variables—such as the direct reduction ratio, moisture content, and oxygen enrichment—introduce multiple solutions, complicating identification of an optimal one.

Benchmarking Conventional BF: However, the ratios of direct reduction (endothermic), CO reduction (exothermic), and H_2 reduction (endothermic) mutually affect CR and PCR but do not directly influence net heat consumption, as their associated reaction heats are internally balanced by heat transfer within the furnace. Therefore, although conventional BF was represented by Conv.BF in Table 3, it is considered acceptable in comparing heat consumption and CO_2 emissions. Note that this also applies to the heat of fuel gasification (endothermic reaction): when top gas is reused outside the system, the heat of gasification must be accounted for as heat consumption on the heat-supply side (i.e., the BF).

(2) Cases to be evaluated

The comparison covers two main scenarios: (1) a conventional BF (Conv.BF; CR = 300 kg/thm) and (2) SimpLE BF—four cases: S.BF-1 (PC with LV coal), S.BF-2 (PC with HV coal char), S.BF-3 (no PC), and S.BF-4 (same as S.BF-3 with green H_2). All cases are evaluated on the effects of energy savings and CO_2 reduction under identical furnace volume, production rate, and internal pressure. Raw materials and operating conditions are listed in Tables 1 and 2.

Table 1. Compositions of ore and products

Pig iron		Slag		Sinter	
Fe	94.8%	SiO_2	35%	T.Fe	57.2%
C	4.5%	Al_2O_3	15%	FeO	7.4%
Si	0.4%	CaO	45%	Fe_2O_3	73.7%
Mn	0.2%	MgO	5%	Others	18.9%
P	0.1%				

Table 2. Compositions of carbonaceous materials

	Coking coal	LV coal	HV coal	Coke	LV-Char	HV-Char
C	80.3%	80.2%	76.8%	87.5%	85.5%	92.1%
H	4.7%	3.8%	5.7%	0.1%	0.5%	0.5%
O	4.8%	3.1%	12.2%	0.0%	0.0%	0.0%
N	2.1%	2.3%	2.0%	1.5%	2.3%	1.6%
Ash	8.1%	10.5%	3.4%	10.8%	11.7%	5.8%
FC	64.9%	74.5%	54.3%			
VM	27.0%	15.0%	42.3%			
LHV(MJ/kg)	32.10	31.58	30.85	29.73	29.52	31.75

(3) Operational Feasibility

Table 3. Operation figures of blast furnaces; Conventional BF vs. SimpLE BF

		Case	Unit	Conv.BF	S.BF-1	S.BF-2	S.BF-3	S.BF-4
Process Input	Top charge burden	Sinter ratio	%	85	85	85	85	85
		Sinter + Ore	kg/thm	1663	1663	1663	1663	1663
		Coke	kg/thm	300	**57**	**57**	**167**	**167**
	Hot blast, Oxygen	Temperature	℃	1200	25	25	25	25
		Oxygen	Nm^3/thm	50	**154**	**135**	**104**	**103**
		Air	Nm^3/thm	901	—	—	—	—
		Moisture	g/Nm^3	19	—	—	—	—
	Injection fuel	Pulver. carbon	kind	LV coal	LV coal	HV **char**	—	—
		PC rate	kg/thm	200	**200**	**131**	0	0
		Tar/light oil	kg/thm	0	10	26	16	16
	Gas reforming fuel & agent	**COG**	Nm^3/thm	N/A	62	145	100	100
		CH_4 or H_2	Nm^3/thm	N/A	CH_4;49	CH_4;49	CH_4;108	**H_2;375**
		Steam	kg/thm	N/A	39	40	0	0
		Air	Nm^3/thm	N/A	0	0	38	0
		Oxygen	Nm^3/thm	N/A	7	19	46	14
	3-Stage Tuyere Blown-in gas	**OD**	÷	N/A	nearly 0 (H_2O, CO_2: nearly 0 vol%)			
		3rd stage	Nm^3/thm	N/A	123	193	270	319
			℃		900	900	900	900
		2nd stage	Nm^3/thm	N/A	414	459	612	697
			℃		1300	1300	1300	1300
		1st stage	Nm^3/thm	N/A	300	330	302	380
			℃		1300	1300	1300	1300
Process Output	Slag rate		kg/thm	304	**252**	**225**	**233**	**233**
	Heat loss (Furnace)		MJ/thm	420	420	420	420	420
	Bosh gas	Flame temp.	℃	2207	2440	2430	2483	2393
		Volume	Nm^3/thm	1348	**500**	**500**	**500**	**550**
	Top gas	Volume	Nm^3/thm	1540	**1264**	**1289**	1415	1626
		TGR ratio	—	N/A	0.76	0.75	0.78	0.80
		Temperature	℃	164	125	151	137	181
	Process temperatures	**Point W**	℃	952	888	892	880	852
		Point M	℃	763	668	694	662	646
		Red. start	℃	731	**600**	**652**	**600**	**600**
		Red. end	℃	(1400)	**888**	**892**	**896**	**898**
Direct reduction ratio			%	33.0	**0.0**	**0.0**	**0.0**	**0.0**
CO reduction ratio			%	60.2	63.7	62.8	58.4	40.0
H_2 reduction ratio			%	6.8	36.3	37.2	41.6	60.0
Shaft efficiency			%	90	93	**95**	**95**	79
Heat flow ratio at shaft top			—	0.84	**0.83**	**0.80**	**0.81**	**0.73**

Heat and Mass Balance Results: Table 3 summarizes the operational figures for a conventional BF (Conv.BF) and four SimpLE cases (S.BF-1 to -4). Smart Reduction (600–900 °C reduction) proved applicable to all SimpLE cases to realize ultra-low CR operation (CR = 57–167 kg/thm), utilizing COG, NG (CH_4), and hydrogen.

Reforming Agent Selection: Reforming is adiabatic and thus not a heat loss, whereas CO_2 separation is a heat loss. Therefore, reforming agents should be selected in order of

priority based on their lower CO_2 emissions: steam, oxygen, then CO_2. Accordingly, steam was applied in S.BF-1 and S.BF-2. Oxygen was chosen in S.BF-3 due to the high reforming load on the hot stove. In S.BF-4 without methane reforming, the TGR ratio was increased to compensate for the endothermic heat of hydrogen reduction.

Thermodynamic Verification (Rist Diagram): Fig. 7 presents the Rist diagram for S.BF-1 alongside Conv.BF. The SimpLE operating line (ABPE line) is steeper than that of Conv.BF due to the inclusion of recycled top gas. However, the external fuel rate actually reduces greatly independent of shaft efficiency (Table 3), because effective gas utilization approaches 100% by TGR and hot-stove fuel usage. This analysis demonstrates the thermodynamic feasibility and distinct features of SimpLE BF.

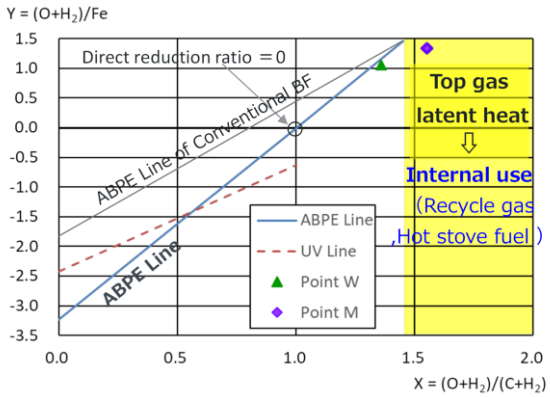

Figure 7. Rist diagram(S.BF-1)

Validation: These analyses demonstrate the feasibility of ultra-low CR operation and highlight key structural differences compared to the conventional BF.

3.2 Evaluation of Heat Consumption and CO_2 emissions

This section compares the heat balance of the BF alone first, including the energy required for CO_2 separation (De-CO_2). Subsequently, the net heat consumption across the entire ironmaking section is evaluated. This includes the coke oven (carbonization and gas purification), the sintering machine with integrated denitrification, and the BF. Preconditions for the comparisons are summarized in Table 4.

Table 4. Preconditions of heat balance calculation

	Oxygen production	Hot blast compressor	De-CO_2 heat	N_2, Plant air, Water	Sintering agent	Tar/oil	Surplus gas*2
Conv.BF	0.6*1 kWh/Nm^3	0.1 kWh/Nm^3	2 GJ/tCO_2	No count in the paper	Fine coke	For sale, no count for CO_2	to downstream /power plant
SimpLE BF	0.5*1 kWh/Nm^3	depending gas density*1			Fine coke Char	Tuyere injection	No surplus gas

*1) Assuming outlet pressure is proportional to gas density
*2) All carbon in the surplus gas including BOF gas is counted as CO_2 emissions.

(1) Heat Balance of the Blast Furnace alone

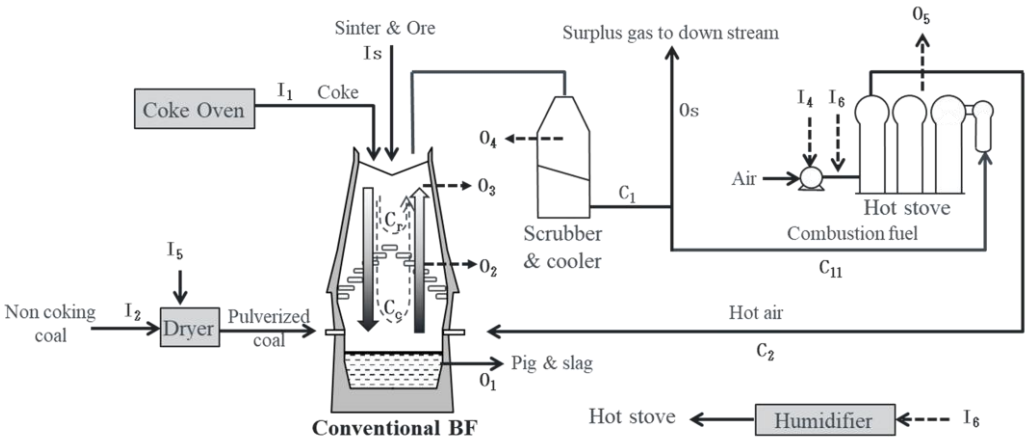

Figure 8. Process/heat flow of Conventional BF

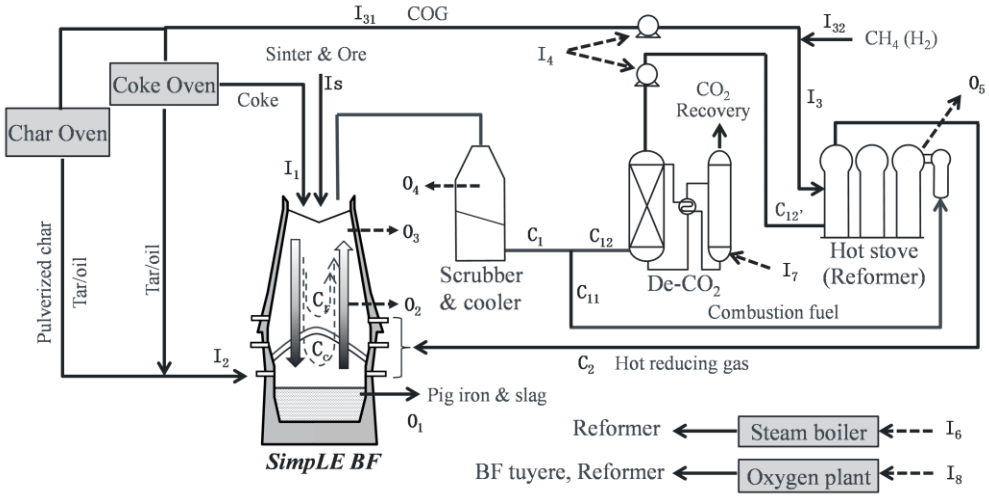

Figure 9. Process/heat flow of SimpLE BF

BF-Internal Energy Flows: The energy flow within the BF is illustrated in Fig. 8 (Conventional BF) and Fig. 9 (SimpLE BF). As shown in Fig. 8, conventional BF releases surplus gas (Os) from the system. In contrast, Fig. 9 shows that SimpLE BF creates a closed loop where top gas is decarbonated (I_7) and recycled (C_{12}), eliminating surplus gas export. The symbols in the flow diagrams and net heat consumption values (O_1–O_6) are summarized in Table 5.

Table 5. Heat balance in blast furnaces (Unit: GJ/thm)

			Conv.BF	S.BF-1	S.BF-2	S.BF-3	S.BF-4
BF-Input	Is	Sinter	0.62	0.53	0.49	0.51	0.51
	I_1	Top charge fuel	8.92	1.69	1.69	4.96	4.96
	I_2	Tuyere inject. fuel	6.32	6.70	5.12	0.59	0.59
	I_3	Supplementary fuel	0	2.93	4.54	5.79	5.97
	I_{31}	COG (Reforming)	N/A	1.18	2.77	1.93	1.93
	I_{32}	CH_4 or H_2(S.BF-4)	N/A	1.74	1.76	3.86	H_2;4.04
	I_4	Main Blower - TRT	0.22	0.11	0.13	0.17	0.19
	I_5	Dryer	0.23	0.23	N/A	N/A	N/A
	I_6	Humidifier/Boiler	0.03	0.12	0.13	N/A	N/A
	I_7	De-CO_2 heat	N/A	0.97	0.94	0.91	0.64
	I_8	O_2 plant (cryogenic)	0.11	0.29	0.28	0.27	0.21
	SUM		16.4	13.6	13.3	13.2	13.1
BF-internal	C_1	Top gas	5.52	7.93	8.15	8.02	11.67
	C_{11}	H/S comb. fuel	1.83	1.87	2.07	1.79	2.31
	C_{12}	TGR/ Surplus-gas	3.70	6.06	6.08	6.23	9.35
	C_2	Hot air/ reducing gas	1.65	1.31	1.55	1.92	2.23
	Cc	Preheat of coke/char	0.55	0.12	0.12	0.36	0.36
	Cr	Generated gas s.heat	0.37	0.32	0.33	0.32	0.31
BF-Output	O_1	Pig iron & slag	11.17	10.99	10.91	10.94	10.94
	O_2	H.L.(BF body)	0.42	0.42	0.42	0.42	0.42
	O_3	H.L.(Burden water)	0.08	0.07	0.07	0.07	0.08
	O_4	H.L.(Top gas)	0.30	0.18	0.24	0.23	0.36
	O_5	H.L.(Hot stove)	0.18	0.19	0.21	0.18	0.23
	O_6	H.L.(Utility);I_4 to I_8	0.58	2.10	1.90	1.85	1.53
	Os	Surplus gas	3.70	0.00	0.00	0.00	0.00
	SUM		16.4	13.6	13.3	13.2	13.1
Net heat consumption of BF			12.7	13.6	13.3	13.2	13.1

Note) TRT: Top pressure recovery turbine

Net Heat Consumption Analysis (Table 5): The net heat consumption of SimpLE BF appears higher due to CO_2 separation energy (I_7) and oxygen production (I_8), which accounts for the differences among S.BF-1 to -4. Excluding I_7, however, lowers it below the Conv.BF level. This reduction is attributed to: (1) lower sensible heat losses due to reduced top-gas volume and slag generation, (2) lower blower power demand due to reduced gas density, and (3) effective use of top gas latent heat offsetting the endothermic fuel

decomposition.

(2) Net Heat Consumption of the Ironmaking Section

Comparison with Conv.BF: Fig. 10 compares the net heat consumption of the entire ironmaking process (including coke making and sintering). SimpLE BFs achieve comparable or lower net heat consumption than Conv.BF. This indicates that the energy penalty for CO_2 capture is effectively compensated by the process efficiency improvements in the BF and the reduced energy demand in upstream processes (coke ovens) due to the ultra-low coke rate.

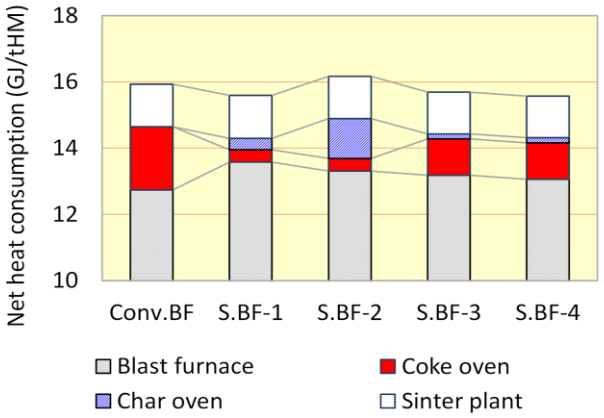

Figure 10. Net heat consumptions of ironmaking

Comparison among S.BF-1 to -4: In S.BF-2, the heat to carbonize HV coal causes a slight increase of 2% (0.3 GJ/thm) from Conv.BF. In contrast, S.BF-4 shows the lowest net heat due to enhanced H_2 reduction. However, H_2 production requires 5 kWh/Nm³, and liquefaction, transport, and storage incur about 30% energy loss [32], leading to an additional 5.6 GJ/thm (net) and 23 GJ/thm (gross) outside the main balance. Then, the total gross heat consumption becomes approximately 2.4 times that of Conv.BF.

(3) Total Input C and CO_2 emissions

Fig. 11 shows the total CO_2 emissions including surplus gases, assuming utilities (e.g., oxygen and electricity) and downstream energy are replaced by CN sources.

In SimpLE cases (S.BF-1 to -3), "ultra-low CR, surplus gas usage, and low-C fuel (CH_4)" reduce Input C by 37–41% compared to Conv.BF. Since SimpLE incorporates De-CO_2, the total reduction reaches 58–62%

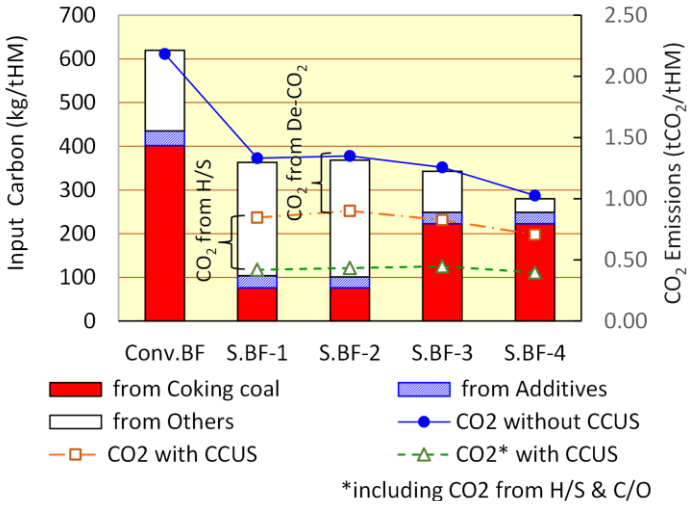

Figure 11. Input C and CO_2 emissions of ironmaking

with CO_2 recovery. In S.BF-4 (green H_2), the reduction reaches 53% for Input C and 68% for CO_2 emissions with CO_2 recovery. Furthermore, oxygen combustion of the N_2-free hot stove exhaust gas (Fig. 9; C_{11}) allows for efficient capture of an additional ~15% of emissions, potentially achieving a total reduction of ~75%.

4. Challenges of Ultra-Low CR Operation

4.1. Pulverized Coal (PC) Combustion Efficiency

(1) Combustion Rate of Solid Particles and Rate-Controlling Factors

Combustion Mechanism: For ultra-low CR operation, avoiding coke pulverization (typical in conventional raceways) is essential to establish a preferential PC combustion over coke. This study evaluates the concept introduced in Section 1: reducing the blast velocity suppresses coke pulverization and thereby enhances preferential PC combustion.

Model Framework: Following Ohno et al. [14], the combustion and gasification rates of solid particles in the raceway are described using an overall rate coefficient (K_{all}) that aggregates the effects of chemical reaction (K_c), film diffusion (K_f) and turbulent diffusion (K_t). The volumetric reaction rate R is governed by the particle-flow characteristics (Eqs. (1)–(2)), with rate coefficients defined in Eqs. (3)–(6).

$$r = K_{all} \cdot C_{\_o2} \qquad (1)$$

$$R = Ws/Vg \cdot 6/(\rho_p \cdot D_p) \cdot K_{all} \cdot C_{\_o2} \qquad (2)$$

$$1/K_{all} = 1/K_c + 1/K_f + 1/K_t \qquad (3)$$

$$K_c = 6.5 \times 10^5 \cdot T^{0.5} \cdot exp(-22000/T) \qquad (4)$$

$$K_f = 3.65 \times 10^{-4} \cdot (T/273)^{1.75}/(D_p \cdot P) \qquad (5)$$

$$K_t = 3.6 \times 10^{-2} \cdot F_k \cdot V \cdot \rho_p \cdot D_p \cdot (U_f/D_f) \qquad (6)$$

$$V = V_g/Ws \qquad (7)$$

(where K_{all}: Overall reaction rate coefficient, $C_{\_O2}$: Oxygen concentration, T: Temperature (K), P: Absolute pressure, V_g: Gas flow rate, W_s: Particle flow rate, ρ_p: Particle density, D_p: Particle diameter, K_c: Chemical reaction rate coefficient, K_f: Film diffusion rate coefficient, K_t: Turbulent diffusion rate coefficient, F_k: K_t correction factor, U_f: Flame speed, D_f: Flame diameter, V: Gas volume per unit mass of particle

mass.)

Assumptions: The analysis incorporates the following assumptions:

1. **High-Temperature Kinetics:** At temperatures of approximately 2000 °C or higher, combustion is not limited by chemical kinetics (K_c) [14,33].
2. **Lump Coke Reaction:** The reaction rate of lump coke is controlled by gas film diffusion (K_f) both inside and outside the raceway [14].
3. **PC Reaction within Raceway:** The governing diffusion mechanism depends on the furnace type [14]. PC particles are governed by turbulent diffusion (K_t) in oxygen BFs(SimpLE), whereas they are governed by a combination of film diffusion (K_f) and turbulent diffusion (K_t) in conventional BFs.
4. **PC Reaction outside Raceway:** In the packed bed, strong mixing caused by repeated collisions with lump coke makes gas-film diffusion (Kf) dominant rate-controlling factor for all BF types [34].

(2) Combustion Reactions Inside and Outside the Raceway

Table 6. Competition for 1 mole of oxygen(O) between PC(C) and coke(C)

	Unit	Total (O) supply	Consumed (C) in raceway	Consumed (C) outside raceway
PC	mol/molO	$x+z_{pc}$	x_1+z_{1pc}	x_2+z_{2pc}
Coke	mol/molO	$y+z_{ck}$	y_1	y_2+z_{2ck}
Combustion efficiency	—	$\eta_{pc}=(x_1+x_2+z_{pc})/(x+z_{pc})$	$\eta_{1pc}=(x_1+z_1)/(x+z_{pc})$	$\eta_{2pc}=(x_2+z_{2pc})/(x+z_{pc})$

Stoichiometry (Table 6): PC competes for combustion with lump coke, circulating coke, and coke dust (CKD) in both the raceway and packed bed [16,20,35]. Table 6 summarizes the molar carbon consumption of PC and coke per mole of blast oxygen (O), distinguishing between the raceway and packed bed regions. The analysis relies on the following definitions and assumptions:

1. **Carbon Input (*x, y*)**: x and y denote the molar carbon input(mol-C/mol-O) from PC and coke, respectively ($x + y = 1$). The subscripts 1 and 2 distinguish the raceway and packed bed zones, respectively.
2. **Extra-O (z)** : z represents oxygen from non-gaseous sources per mole of O, categorized by origin into z_1 (solid O in PC) and z_2 (O from Blast H_2O/CO_2), where

$z = z_1 + z_2$. It is simultaneously classified by consumption into z_{pc} (for PC) and z_{ck} (for coke), where $z = z_{pc} + z_{ck}$.

3. **Oxygen Distribution:** Within the raceway, PC is assumed to fully consume z_1. Outside the raceway, z_2 is distributed based on the preferential combustion fractions $\boldsymbol{\zeta_{2pc}}$ and $\boldsymbol{\zeta_{2ck}}$ —defined as $x_2 / (x_2 + y_2)$ and $y_2 / (x_2 + y_2)$, respectively.
4. **PC combustion efficiency ($\boldsymbol{\eta_{pc}}$):** The PC combustion efficiency $\boldsymbol{\eta_{pc}}$ is defined as the ratio of combusted carbon in the PC. And the following equation applies:

$$\eta_{pc}=(x_1+x_2+z_{pc})/(x+z_{pc})=(1-y_1-y_2+z_{pc})/(x+z_{pc}) \quad (8)$$

$$z_{pc} = z_1+\zeta_{2pc}.z_2 \quad (9)$$

$$z_{2ck} = (1-\zeta_{2pc}).z_2 \quad (10)$$

$$\zeta_{1pc}=x_1/(x_1+y_1) \quad (11)$$

$$\zeta_{2pc}=(x_2+\zeta_{2pc}.z_2)/(x_2+y_2+z_2) \quad (12)$$

Note: ζ_{2pc} in Eq. (12) is determined iteratively. Eq. (8) implies that increasing η_{pc} under fixed conditions (x, z) necessitates reducing coke combustion ($y_1 + y_2$). This reflects the long-standing concern over the combustibility of PC [35], and highlights the intrinsic difficulty of improving η_{pc} while maintaining raceway functions.

(3) Derivation of PC Combustion Efficiency Formula

Coke Fragmentation Mechanism: Coke fragmentation in the raceway is driven by blasting energy. According to Yamaoka et al.[25], coke dust (CKD) generation within the raceway is proportional to the kinetic energy of coke particles colliding with the raceway wall. Based on this, the following assumptions are made:

1. Coke fragmentation is assumed to follow Rittinger's law, where grinding energy is proportional to the generated surface area.
2. The impact energy of swirling coke scales with tuyere blast energy $(\rho_g \cdot U_f^2)^{1/1.3}$ [25].
3. Under constant blast conditions, increasing PCR (decreasing CR) from an all-coke baseline increases the blast energy per unit of coke in proportion to 1/y.

Blast Energy: Defining E_b as the blast energy per mole of oxygen atoms, the energy balance yields:

$$(E_b/y)^{1/1.3} = C_{ck} \cdot (1/Dp_{1ck} - 1/Dp_{ck}) = \left(P'/P \cdot T/T' \cdot (U_{b0}/U'_{b0})^2 \cdot E'_b/y\right)^{1/1.3} \quad (13)$$

where C_{ck} is a material constant, and the right-hand side reflects the reference blast conditions (E_b', U_{b0}', p', T').

From the experimental results for all-coke operation (y = 1), the fragmented coke size in the raceway is expressed as $Dp_{1ck} \approx \omega_1 \cdot Dp_{ck}$ （$\omega_1 \approx$ 0.5～0.7, P'=0.1, T'=1693） [16]. Substituting this relation into Eq. (13) determines C_{ck}, yielding:

$$Dp_{1ck} \approx Dp_{ck}/((1/\omega_1 - 1) \cdot (0.1/P \cdot T/1693 \cdot (U_{b0}/U_{b0}')^2/y)^{1/1.3} + 1) \quad (14)$$

This equation indicates a strong correlation between tuyere blast velocity and fragmented coke size. Although unobserved in Reference [18], this discrepancy likely stems from measurement differences (swirling coke size vs. mean crushed coke size) and the exclusion of coke dust. Consequently, ω_1 is expected to be slightly lower than the experimental value. These hypotheses are validated by the consistency between calculated results and extensive actual measurements. The same validation approach applies to the subsequent analysis.

Preferential PC Combustion in Packed Bed: Assuming adjacent PC and coke particles share identical local gas conditions, the reaction rate ratio of PC to Coke ($RR_2 = R_{2pc}/R_{2ck}$) is derived using Eqs. (2) and (5), where R_{2pc} is PC combustion rate and R_{2ck} is coke combustion rate. Applying the correction coefficient Crr_2 yields:

$$RR_2 = Crr_2 \cdot (\rho_{\gamma\_2pc}/\rho_{\gamma\_2ck}) \cdot (\rho_{p\_ck}/\rho_{p\_pc}) \cdot (Dp_{2ck}/Dp_{2pc})^2 \quad (15)$$

Here, ρ_γ (W_s/V_g) is the particle density per unit gas volume, and ρ_{γ_2pc} denotes the local PC density in the combustion zone within the packed bed. Per 1 Nm^3 of oxygen, the average PC mass in the zone is approximated by $(2-\eta_{1pc}-\eta_{pc})/2 \cdot X$, while the average gas volume is approximated as: $(P/P_0) \cdot (T_0/T) \cdot (\eta_1 + 11.2 \cdot C_{pc\_HN} + 1/C_{tg_{O2}})$, where η_1($= \eta_{1pc} + \eta_{1ck}$) denotes oxygen consumption rate within the raceway. This yields:

$$\rho_{\gamma\_2pc} \approx (2 - \eta_{pc} - \eta_{1pc})/2 \cdot X \cdot (P/P_0) \cdot (T_0/T)/(\eta_1 + 11.2 \cdot C_{pc\_HN} + 1/C_{tg\_O2}) \quad (16)$$

The local coke density ρ_{γ_2ck} is derived from the coke particle density ρ_{p_ck} and bed void fraction ε:

$$\rho_{\gamma_{2ck}} = W_{s\_2ck}/V_g \approx \rho_{p_{ck}} \cdot (1 - \varepsilon)/\varepsilon \quad (17)$$

The mean coke size in the packed bed near the raceway, Dp_{2ck} , is defined as the average of raceway coke (Dp_{1ck}) and dispersed coke dust ($\omega_2 \cdot Dp_{1ck}$, *where* $\omega_2 \approx 0.1$[36]):

$$Dp_{2ck} = (1 + \omega_2)/2 \cdot Dp_{1ck} \qquad (18)$$

Preferential Combustion Fraction (PC to Coke): Using the definition of RR_2 and Eq. (12), the preferential combustion fraction of PC in the packed bed (ζ_{2pc})is:

$$\zeta_{2pc} = \psi \cdot \zeta'_{2pc} = \psi \,/\, (1 + 1/RR_2) \qquad (19)$$

where ψ (≤ 1) denotes the PC-O_2 distribution efficiency at the raceway boundary; $\psi = 1$ indicates stoichiometric distribution.

For the raceway, the preferential fraction ζ_{1pc} is estimated assuming the reaction rate ratio in the raceway (RR_1) is proportional (coefficient Crr_1) to that in the packed bed (RR_2):

$$RR_1 = Crr_1 \cdot RR_2 \qquad (20)$$

$$\zeta_{1pc} = 1 \,/\, (1 + 1/RR_1) \qquad (21)$$

Eqs. (8) through (21) thus allow the calculation of PC combustion efficiencies across both zones.

(4) Validation of PC Combustion Rate Estimation Formula

Eqs. (8)–(21) constitute a novel deductive formulation derived from reaction principles (Eqs. 1–7, Table 6). Given the underlying assumptions, the model is validated inductively against extensive experimental data obtained from previous research reports. Table 7 summarizes the results for Cases 1–13, detailing experimental conditions (X to Dp_{ck}), calculation parameters (ε to Ψ), and the comparison between calculated (η_{pc_CAL}) and measured (η_{pc_Actual}) efficiencies.

Assumptions and Parameter Settings:

1. **Physical properties:** Standard values are applied

- $Dp_{pc} = 50\times10^{-6}$ m, $\rho_{p\text{-}ck}$=1000 kg/m^3, $\rho_{p\text{-}pc}$= 400 kg/m^3
- Void fraction ε = 0.45 without raceway shell

2. **Coefficient settings:** determined via model calibration

- ω_1 = 0.5, Ub_0 / Ub_0' = 1 (Eq. (14)), Crr_2 = 1 (Eq. (15)), Crr_1 = 4 (Eq. (20))
- Ψ = 0.8 (atmospheric pressure), 0.9 (pressurized conditions: $P/P_0 \geqq 1.5$)
- Void fraction ε = 0.30 under raceway shell is present

3. **Coke dust (CKD) generation:**

- Pitch Coke (Cases 1–3, 9–11) [19]: CKD generation is neglected.

- BF Coke (Cases 4–8, 12, 13): Generation is proportional to x [17,20], with dust combusting preferentially in the packed bed.

4. Combustion parameters:

- **η_{1pc}:** Reported values are adopted for Cases 9–11; others are estimated based on consistency.

- **Flame Temperature:**

Cases 4–11: Based on reported values

Case-13: Calculated as all-coke operation (minimum PC combustibility)

Others: theoretical adiabatic flame temperature is applied.

- **Coal to oxygen ratio X:**

Cases 1–8: Based on reported values

Cases 12,13: Ditto. X≈ 0.48 is applied as PCR=200 kg/thm [17].

Cases 9–11: Estimated so as to fulfill the experimental conditions [18]

Table 7. Verification of the PC combustion efficiency calculation with various experimental results

	Operating conditions						Calculation variables				Validation		Note
	X	X_G	P/P_0	$C_{tg\text{-}O2}$	T (K)	Dp_{ck} ×10^{-3}	ε	η_{1pc}	CKD %	ψ	$\eta_{pc\_CAL.}$	η_{pc_Actual}	
Case-1	0.8	1.57	1.0	0.6	2373	35.0	0.45	0.20	**0**[*1]	0.8	0.84	0.84	HV
Case-2	1.2	1.57	1.0	0.67	2373	35.0	0.45	0.20	**0**[*1]	0.8	0.52	0.51	X ↑
Case-3	1.2	1.57	2.5	0.67	2373	35.0	0.45	0.31	**0**[*1]	0.9	0.93	0.93	Pressure ↑
Case-4	0.55	1.59	2	0.25	2072	22.5	0.3	0.21	21	0.9	0.92	0.92	HV
Case-5	0.75	1.59	2	0.27	2027	22.5	0.3	0.21	27	0.9	0.79	0.82	X ↑
Case-6	0.9	1.59	2	0.27	1979	22.5	0.3	0.21	32	0.9	0.71	0.69	X ↑
Case-7	0.5	1.64	1.0	0.74	2573	20.0	0.45	0.44	21	0.8	0.80	0.80	HV
Case-8	0.7	1.64	1.0	0.76	2573	20.0	0.45	0.41	25	0.8	0.65	0.65	X ↑
Case-9	0.75	1.57	2–5	0.29	2423	35.0	0.45	0.78[*2]	**0**[*1]	0.9	0.98	0.96	PCR=200, HV
Case-10	1.0	1.57	2–5	0.34	2423	35.0	0.45	0.64[*2]	**0**[*1]	0.9	0.96	0.94	PCR=300, HV
Case-11	0.75	1.41	2–5	0.29	2423	35.0	0.45	0.50[*2]	**0**[*1]	0.9	0.95	0.94	PCR=200, LV
Case-12	0.48	1.63	1.0	0.21	2273	17.0	0.3	0.47	+20	0.8	0.49	0.49	HV
Case-13	0.48	1.22	1.0	0.21	2643	17.0	0.45	0.00	+23	0.8	0.12	0.02	LV, Ash=0.5%
Case-14	1.47	3.6	1.0	0.33	1773[*3]	50.0	0.3	**0**[*3]	**0**[*3]	**0.99**	**0.99**	**0.99**	Direct melting furnace
Case-15	1.38	1.38	4	0.6	2773	35.0	0.45	**0**[*3]	**0**[*3]	**0.9**	**0.89**	N/A	S.BF-1, LV
Case-16	1.16	1.16	4	0.6	2773	35.0	0.45	**0**[*3]	**0**[*3]	**0.9**	**0.89**	N/A	S.BF-2, HV char
Case-1'	0.80	1.49	1.0	0.62	2973	35.0	0.45	0.20	30	0.8	0.60	N/A	Scrap melter

Note) *1: Pitch coke effect, *2: Pitch coke effect (measured values), *3: Raceway-free effect
*4: Measured

Verification Cases:

1) Cases 1–3 (Yamaoka et al. [15,37])

Atmospheric/pressurized oxygen combustion tests using pitch coke (25–50 mm). Note that PC combustion efficiency (η_{pc}), originally evaluated on a volatile matter basis, was converted to a carbon basis in Table 6 (and for Cases 4–6, 12, 13). Calculated results match the experimental trends: $\eta_{pc} \geq 80\%$ at atmospheric pressure ($X \leq 0.8$) and $\eta_{pc} \geq 90\%$ at 0.25 MPa ($X \leq 1.2$). In Fig. 12, calculated results for P = 0.1 and 0.25 MPa are shown as solid lines. These curves effectively capture the central tendency of the extensive experimental scatter plots reported in [15,37]. Table 7 exemplifies specific data points from these datasets, further confirming the quantitative agreement.

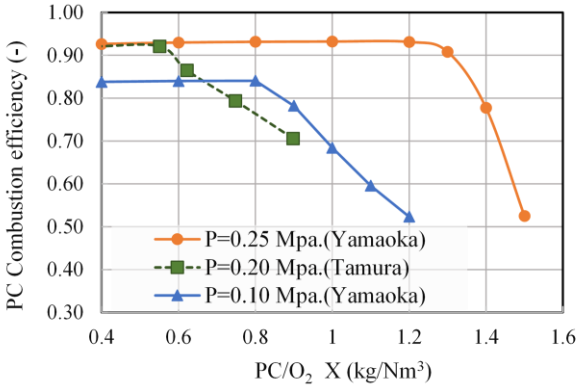

Figure 12. PC combustibility against X (Coal/O_2)

2) Cases 4–6 (Tamura et al. [13])

Pressurized (0.2 MPa) hot air tests using BF coke (20–25 mm). The experimental conditions—coke type and size, oxygen concentration, combustion temperature, etc.—differ significantly from Cases 1–3. Crucially, a low-permeability shell was observed near the raceway, so $\varepsilon = 0.30$ was applied. Ψ was set to 0.9, as with Case 3 ($P = 0.25$ MPa). The calculated results, shown as the dotted line in Fig. 12, exhibit excellent agreement with the extensive experimental data reported in [13] across a wide range of X = 0.39–0.9. Table 7 lists three representative cases (Cases 4–6) to exemplify this quantitative consistency. Comparisons used measurements (η_{pc_Actual}) at 700 mm above the raceway to exclude errors from gasification by CO_2 in the oxygen-excessive zone ($X < 0.63$).

3) Cases 7-8 (Ohno et al. [14])

Atmospheric oxygen combustion using BF coke (15–25 mm). Calculations assume a burner configuration (Type D) that enhances PC-O_2 mixing. Despite differences in coke type and the use of CO_2 for tuyere-tip temperature control, calculated results align well with experimental values.

4) Cases 9–11 (Yamagata et al. [18])

Pressurized hot air tests using BF coke (20–50 mm)— conditions inferred from the timing, affiliation, and pressurized vessel usage. η_{1pc} adopts experimental measurements, while $\eta_{pc\ Actual}$ refers to simulation values from the report. Calculated results align well with literature values.

5) Cases 12-13 (Ariyama et al. [17])

Atmospheric hot air tests with BF coke (≈17 mm). Case 12 and Case 13 correspond to HV coal (Coal-A) and LV coal (Coal-D), respectively. Assumptions include $\varepsilon = 0.30$ for Case 12 (with raceway shell) and $\varepsilon = 0.45$ for Case 13 (without shell). The model accurately captures the sharp efficiency drop with LV coal. Furthermore, applying pressure conditions to these models yields improvements (89% and 67%) comparable to actual BF operations [38,39].

(5) Evaluation of the Estimation Formula and Application to SimpLE BF

Model Accuracy and Consistency: The proposed model (encompassing Eqs. 8-21) reproduces both the trends and absolute values of PC combustion efficiency across diverse conditions (Fig. 12, Table 7). Deviations are mostly within ±3%, and the error is limited to 10% even under the extreme condition of Case 13 ($\eta_{pc} = 0.02$). This confirms the model's high consistency.

Parameter Sensitivity: Although η_{1pc} was estimated for cases without reported data (except Cases 6–8), its influence is minor. For example, a +10% change in η_{1pc} alters η_{pc} by only +2%, +4%, and +1% in Cases 1, 2, and 3, respectively. Therefore, the consistency across a wide range of X in Fig. 12 results from the model's validity, not from arbitrary parameter tuning.

Validation of Reducing Blast Velocity (Case 14): The blast velocity is not evaluated in Cases 1-13 due to "Assumptions and Parameter Settings 2. ($Ub_0 / Ub_0' = 1$)". But the effect of low blast velocity—raceway-free operation—is strongly supported by Shibaike et al. [40]. Fine carbonaceous dust (≈0.06 mm) combusted in an atmospheric 300 mm-bed-height BF-coke (40-60 mm) without raceway (blast velocity≈28 m/s) achieved η_{pc} of 98.5% for $X = 1.47$ (equivalent to $X \approx 0.6$ as PC [14]). Despite stoichiometry more severe than Case-12

(where X≈0.48, η_{pc} = 49% with unburnt carbon of 51%), the unburnt ratio in Case-14 (1.5%) was reduced to 1/34. This serves as direct evidence that eliminating the raceway drastically improves PC combustion.

Governing Mechanism without Raceway: In Case-14, the kinetic reaction rate ratio (RR_2) is calculated as ≈ 68 (Eq. 15), implying that η_{pc} should kinetically approach 100% before coke consumption. The measured η_{pc} of 98.5% thus indicates that physical distribution, not kinetics, is the limiting factor. The efficiency 98.5% can be interpreted as a direct measure of the PC-O_2 distribution efficiency ($\Psi \approx 0.985$) under low-velocity blast conditions. This is reinforced by other results in the same study [40]: carbon consumption rates correlated with dispersibility—LPG (gas, 99.5%) > Dust (98.5%) > Plastics (0.7 mm, 95.7%). These findings strongly imply that physical mixing and fuel's physical properties are the dominant rate-limiting factors in low-velocity packed-bed combustion.

Theoretical Basis of Ψ: PC-O_2 distribution efficiency Ψ is determined primarily by pressure (affecting velocity u) and not by the geometry of the tuyere or PC lance. This is explained phenomenologically by the Peclet number ($Pe = u \cdot L/D_z$, *where* u: actual gas velocity, L: representative length, D_z: mixed diffusion coefficient) as in the following equation:

$$\Psi = 1/(1 + \alpha_p \cdot Pe) \qquad (22)$$

, where α_p: correction factor, $Pe \ll 1$ under strong forced mixing by the packed bed. Given that mixed diffusion $D_z \approx D_t = u' \cdot L$ (where u' is fluctuation velocity of turbulence) [34,41,42], Pe becomes a function of u/u'. Considering $u \propto T/P$, Ψ improves (approaches 1) under high pressure or low velocity, independent of particle size L or any other factors—secondary dependence via u' remains a subject for future study.

Avoidance of Raceway Shell: Table 7 infers that the theoretical combustion temperature above 2373 K (2100 °C) can prevent the formation of a raceway shell, which depends on the ash content of PC and the melting point of coke fines [13].

Application to SimpLE BF: Applying these findings, η_{pc} for SimpLE (Cases 15-16) is estimated at the PC gasification limit ($X = X_G$). Shell formation is prevented by maintaining $T > 2373$ K ($\varepsilon = 0.45$). Low-velocity blast (e.g. U_{b0} =100) realizes raceway-free combustion, which means $y = 1$ (no swirling/crushing), $CKD = 0\%$, $\eta_{1pc} = 0$, and high Ψ. Adopting Ψ =

0.9—very conservative under pressurization compared to 0.99 under atmospheric pressure in Case-14—still achieves η_{pc} = 0.89 with unburnt PC < 9 kg/thm. Conversely, assuming raceway formation with the same U_{bo} would drop η_{pc} to ~2%.

4.2 Mechanism of Unburnt PC Consumption Under Ultra-Low CR Conditions

(1) Conventional Unburnt PC consumption mechanism

In conventional BFs, unburnt PC (C) is prevented from discharging by the following two main mechanisms:

[A] Direct reduction by liquid FeO (FeO + C → Fe + CO);

[B] Gasification reactions by CO_2 or H_2O (e.g., CO_2 + C → 2CO) generated through gas-based reduction (e.g., CO + FeO → CO_2+Fe) [12,43].

However, in SimpLE BF, where the gas-based reduction ratio reaches 100% (OD ≈ 0), these mechanisms are inoperative. This necessitates a "third mechanism" to suppress unburnt PC discharge.

(2) The third Unburnt PC consumption mechanism

Evidence from Pilot-Scale Scrap Melting (Fig. 13): The existence of the third mechanism is strongly supported by the pilot-scale scrap-melting test by Kamei et al. [44]. They converted the experimental blast furnace used in Case-1 into a scrap-melting furnace (Fig. 13) and operated it with BF coke under conditions analogous to SimpLE: CR = 150 kg/thm, PCR = 140 kg/thm (X = 0.8), and a bosh gas rate of 550 Nm³/thm with OD = 0. As illustrated in Fig. 13, coke (20–50 mm) was charged in a fully mixed state with scrap. Although the original report did not explicitly discuss the "cohesive zone structure," this full-mixing configuration inevitably forms a coke-slit-less cohesive layer effectively identical to Smart Charging.

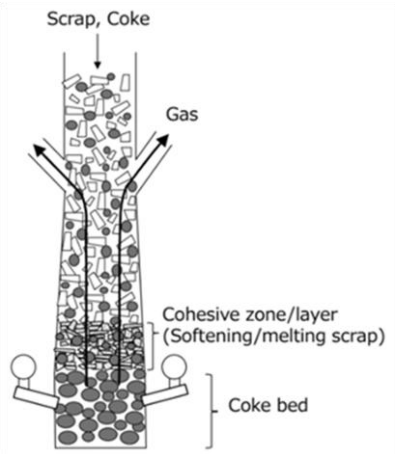

Figure 13. Scrap melting furnace (Image)

Evidence of In-Furnace Filtration: As shown in Table 7 (Case-1'), the use of BF coke—instead of pitch coke in Case-1—resulted in a lower η_{pc} =60% (instead of 84%), theoretically

generating significant unburnt PC (40%, or 44 kgC/thm). Since conventional consumption mechanisms [A] and [B] were inactive (Scrap RD=100%, Bosh gas *OD*=0), this unburnt PC should have been emitted as top dust. However, the actual dust emission, calculated from the carbon balance shortage, was less than 4 kgC/thm (1–2 wt% of fuel rate)—obviously less than that of all-coke operation. This rationally identifies the dust as coke fines rather than unburnt PC, implying unburnt PC emission was negligible. This discrepancy serves as experimental proof that unburnt PC—having a terminal velocity < 0.1 m/s—was entrained by the bosh gas (~4 m/s) or washed by dripping metal, and subsequently filtered (trapped) within the mixed-burden cohesive zone.

Consumption Balance and Stability: Carbon balance analysis confirms that the trapped unburnt PC (44 kgC/thm) was fully consumed within the furnace. Based on the estimated η_{pc} = 0.60, the carburization rate ratio (unburnt PC to coke) is calculated as $RR_3 \approx 0.5$, implying that the trapped PC was consumed 50% by carburization and 50% by re-combustion. The operation remained stable regarding permeability and tapping [44], proving that unburnt PC—unlike coke dust—does not impair the gas or liquid permeability of the lower furnace [36,45,46].

Thermodynamic and Physical Advantages: Furthermore, this consumption mechanism facilitates hot gas flow to the furnace center. This is because (1) the heat required for carburization or combustion is significantly lower than that for direct reduction or gasification, and (2) unburnt PC does not degrade coke bed permeability unlike coke dust.

Applicability to SimpLE BF: These findings directly apply to the lower furnace of SimpLE BF, where a coke-slit-less cohesive zone is formed via Smart Charging (full-mixed charging) and the thermal load is minimized (only melting metallic iron) via Smart Reduction. This configuration realizes a functional dust filter to utilize unburnt carbon effectively and a mechanism to allow hot gas to reach the furnace center.

4.3 Coke Bed Structural Integrity (Carburization Effect on Coke Size)

(1) Concern of Coke Size in the Lower Furnace

In SimpLE BF, Smart Reduction and Smart Combustion (raceway-free) ensure the supply

of strong, large-sized coke to the lower furnace by preventing gasification and shear-induced degradation. However, in ultra-low CR operation, coke is primarily consumed by carburization. As 10–20 wt% of coke is carburized in the hearth [47], significant size reduction in the coke bed (dripping zone) is a potential concern.

(2) Impact of Carburization

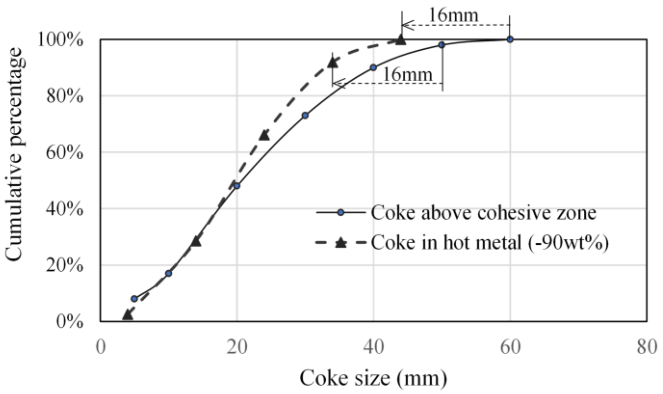

Figure 14. Change in coke size distribution by carburization

Fig. 14 compares the initial coke size distribution above the cohesive zone (solid line) [48] with the estimated distribution after 90% carburization (dashed line). The estimation assumes uniform surface reaction, where the carburization rate dm/dt is proportional to the surface area πD_p^2. Since mass $m \propto D_p^3$, differentiating with respect to time yields $dm/dt \propto D_p^2 \cdot dD_p/dt$. Equating the reaction rate to the mass change ($D_p^2 \propto D_p^2 \cdot dD_p/dt$) reveals that the diameter reduction rate dD_p/dt is constant, independent of particle size. This "uniform shrinkage" implies that smaller particles disappear faster, while larger ones lose only a constant diameter increment.

(3) Resulting Permeability Improvement

Even with 90% mass consumption (corresponding to a uniform diameter reduction of ~16 mm), the arithmetic mean size decreases only slightly (27 mm → 25 mm). Crucially, the harmonic mean size—which governs bed permeability based on specific surface area—actually improves (18 mm → 20 mm). This counter-intuitive result arises because uniform shrinkage eliminates the fine fraction. Additionally, the resulting narrower particle size ratio (max/min) leads to an increase in the void fraction.

Furthermore, if coke is simultaneously consumed by combustion, the consumption time is proportional to the square of the diameter (D_p^2). This accelerates selective consumption of smaller particles, narrowing size distribution and enhancing permeability. Thus, permeability in the coke bed is maintained or improved.

4.4 Gas Permeability in the Furnace Under Ultra-Low CR Conditions

This section evaluates the gas permeability (i.e., pressure drop) inside the furnace after implementing ultra-low coke rate (CR) operations.

(1) Permeability Resistance Coefficient and Pressure Drop in the Shaft

Evaluation Model: Pressure drop ΔP in the shaft (transitional Reynolds number regime) is evaluated using the modified Carman equation (Eqs. 23–26) [21,23,24], which are well applied to practical operations. The permeability resistance coefficient K is a key index, sensitive to particle size D_p and porosity ε.

$$\Delta P = 1 \times 10^{-6} \cdot g \cdot K \cdot J \cdot {u_0}^{2\text{-}\beta} \cdot \Delta L \qquad (23)$$

$$J = {\rho_g}^{1-\beta} \cdot \mu^{\beta} \qquad (24)$$

$$K = K_i \cdot 10^{\alpha \cdot \sigma} \qquad (25)$$

$$K_i = C_k \cdot (\Phi \cdot D_p)^{-(1+\beta)} \cdot (1-\varepsilon)^{(1+\beta)} \cdot \varepsilon^{-3} \qquad (26)$$

(g: gravitational acceleration, u_0: superficial gas velocity, β: correction exponent ≈ 0.3, ρ_g: Gas density, μ: Gas viscosity; see Appendix A for expanded nomenclature)

Particle Size Control: Smart Charging minimizes ΔP via size segregation (controlling the particle size ratio). For example, separating sinter (6–24 mm, avg. 15 mm) into small (6–12 mm) and large (12–24 mm) layers controls the particle size ratio to ≤ 2. This technique increases porosity ε from 40% to approximately 47% [49], significantly reducing K in the lumpy zone (Table 8).

Pressure Drop Reduction (Table 8): Table 8 shows advantages of this control, comparing Conv.BF and S.BF-1 in Table 3. K increases without size segregation, increasing $\Delta P/\Delta L$ by 6% compared to Conv.BF, even though the top gas volume is 18% lower. However, once the layers are separated into small and large ore layers (Smart Charging), the improved porosity significantly lowers the resistance. Consequently, ΔP drops by 24% (at a layer thickness ratio of 1:1) or 34% (at 2:1) compared to the conventional baseline, confirming that strict particle size control is essential for maintaining permeability in ultra-low CR operation.

Table 8. Permeability resistance index and pressure drop in the shaft (lumpy zone)

	Kc_i(Coke layer)	Ko_i(Ore layer)	Thickness ratio	K_L(Lumpy zone)	$\Delta P/\Delta L$
Conv.BF	600[23]	3000[23]	O(v)/C(v)=1.5	2020	Base
S.BF-1	N/A (No coke layer)	3000 (layer-less)	mixed	3000	+6%
		1242 (L), 3057 (S)	(L)/(S)=1	2150	-24%
		1242 (L), 3057 (S)	(L)/(S)=2	1860	-34%

Note） Kc_i: K of coke layer, Ko_i: K of ore layer, K_L: K of lumpy zone

(2) Pressure Drop in the Cohesive Zone

Permeability Resistance of Cohesive Layer (K_{CL}): According to load-softening tests by Kawashiri et al. [25], the conventional K_{CL} ($\approx 100\times Ko_i$) decreases to ~1/10 ($\approx 10\times Ko_i$) for a highly-reduced cohesive layer (RD ≈ 100%), which is derived from suppressing FeO melt formation [23–25]. This applies directly to SimpLE BF. Furthermore, mixing 10–15% coke reduces resistance to < 1/10 [21], attributable to the formation of gas flow paths around coke particles caused by localized carburization and melting of the surrounding metal [22]. Smart Charging (mixing of 4–12 wt% coke) alone lowers K_{CL} to 1/3 to 1/10. Combining both effects, the composite resistance coefficient K'_{CL} is expressed: $K'_{CL} = 1/(1/K_1 + 1/K_2) =$ *(1/13* to *1/20)* $\times K_{CL}$ (K_{CL} of conventional BF) [Factor ①].

Cohesive Zone Thickness (t): The layer thickness t is determined by the balance between the heat transfer rate Q and the thermal requirement of the burden. The heat transfer equation yields:

$$Q = h \cdot a \cdot (A_c \cdot t) \cdot \Delta\theta = p \cdot \Delta H \quad (27)$$

Rearranging for t, and assuming constant productivity p and specific surface area a:

$$t = p \cdot \Delta H / (h \cdot a \cdot A_c \cdot \Delta\theta) = (p/a) \cdot \Delta H/(h \cdot A_c \cdot \Delta\theta) \propto \boldsymbol{\Delta H / (h \cdot A_c \cdot \Delta\theta)} \quad (28)$$

Thickness t depends on enthalpy difference $\boldsymbol{\Delta H}$ (incoming vs. outgoing ore), heat transfer coefficient $\boldsymbol{h}$, gas flow cross-sectional area $\boldsymbol{A_c}$, and mean temperature difference $\boldsymbol{\Delta\theta}$.

$\boldsymbol{\Delta H}$ Reduction: ΔH includes sensible heat, melting heat, carburization heat, and reduction heat. As shown in Table 9, SimpLE BF reduces ΔH to 1/2.8 [Factor ②] by eliminating direct reduction heat, even assuming 50% of the direct reduction heat for Conv.BF. The total ΔH aligns well with the heat flux observed across the cohesive zone (1200–1400 °C) in

Table 9. Heat differences of ore entering and exiting cohesive zone (Unit: kJ/kgFe)

	Sensible	Melting	Carburizing	Reduction	Total ΔH
Conv.BF	224 (200℃)	303	31 (2%C)	1000	1558
S.BF-1	224 (200℃)	303	31 (2%C)	0	558

Fig. 4.

***A_C* Enlargement:** Next, the structural shift from "cohesive layers and coke slits" (Conv.BF) to "single cohesive layer" (S.BF-1) is respectively simplified to Model (a) and Model (b) in Fig. 15. The gas flow cross-sectional area A_{CL} in the cohesive zone is

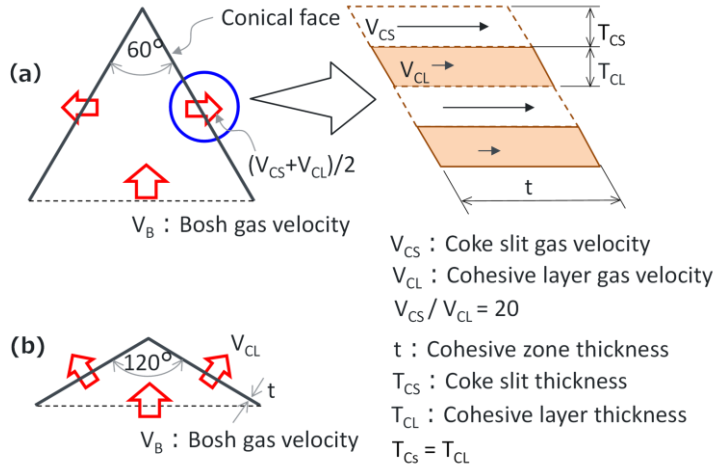

Figure 15. Cohesive zone models for pressure drop calculation
(a) Cohesive zone with coke slit; (b) Cohesive zone without coke slit

geometrically derived as follows, relative to the bosh cross-sectional area A_B: (a) A_{CL}＝0.87･A_B, (b) A_{CL}＝1.15･A_B [Factor ③].

(h·Δθ)* Enlargement:** In Model (a), the permeability ratio between cohesive layer and coke slits—round 1/150 [49]—gives V_{CS}/V_{CL}=20 (see Fig.15). So, the gas velocity in the cohesive zone V_{CL} relative to the bosh gas velocity V_B is: (a) V_{CL}＝0.055･V_B, (b) V_{CL}＝0.87･V_B [Factor ④]. Considering the flow rates, Model (a) is a laminar flow ($h \propto V^{0.8}$) and Model (b) is a transitional flow ($h \propto V^{0.6}$). To estimate ΔP simply and conservatively for S.BF-1, both are regarded as transitional flow. Accordingly, using the bosh gas flow rates shown in Table 10, the heat transfer coefficient ***h for (b) (S.BF-1) is calculated to be 2.9 times greater than that of (a) (Conv.BF). Additionally, the gas temperature in the lower furnace of S.BF-1 is higher than in Conv.BF, resulting in a larger $\Delta\theta$. Thus, it is regarded that ***(h·Δθ)*** is 3 times greater in (b) (S.BF-1) [Factor ⑤].

Thickness (*t*) Reduction: Substituting the above Factors [②③⑤] into Eq. (28), it was concluded that ***t*** in S.BF-1 becomes 1/11 that of Conv.BF [Factor ⑥].

Pressure Drop (*ΔP*) in Cohesive Zone: The pressure drop is determined by integrating the improvements in resistance coefficient [①], gas velocity [④], and zone thickness [⑥]. As shown in Table 10, *ΔP* in S.BF-1 is reduced to **1/10** of Conv.BF. This theoretical estimation aligns with the stable operation of the scrap-melting test [44] (Fig. 13) despite >4 times higher bosh gas velocity than S.BF-1 due to atmospheric pressure and higher fuel rate.

Table 10. Pressure drops at cohesive layer

	Bosh gas (Nm^3/thm)	Passage area	$K_{CL}\times10^{-3}$ (Cohesive layer)	ΔL (Thickness)	ΔP (Cohesive zone)
Conv. BF	1348	Base	300	Base	Base
S.BF-1	500	×1.33	215*1 ×1/13*2	×1/8.4	×1/10

Note) *1: $100\times K_L$ (Table 8), depending on dressing; *2: in case of S.BF-1

(3) Pressure drop of Dripping zone

Zone Definitions and Resistance: In this analysis, the lower furnace is defined as the region below the cohesive zone. Depending on the presence of liquid (slag and metal), it is subdivided into the *"upper" zone** (solid only) and *"lower" zone** [50]. According to Fukutake et al. [50], the pressure drop in the lower* zone accounts for > 50% of the total furnace pressure drop under high-pressure operation (absolute top pressure > 0.28 MPa).

Stability Assessment: In S.BF-1, the pressure gradient in the dripping zone is estimated to be only 1/5 of the conventional level, based on empirical formulae for gas-liquid counter-current flow[51]. This significantly lower gradient suggests the avoidance of operational instabilities such as flooding or coke fluidization[52]. This theoretical stability is consistent with the smooth operation observed in the pilot-scale scrap-melting test[44], verifying the robustness of the lower furnace design.

(4) Total Furnace Pressure Drop

Comparison of Pressure-Drop Head (Fig. 16): Fig. 16 compares the total pressure-drop head (i.e., pressure drop divided by gas density) between Conv.BF and SimpLE BFs under identical furnace geometry and production rates (Table 3). Assumptions include: Top charging is set as O/C of 5.4 for Conv.BF and large/small layer thickness ratio of 1 for SimpLE BFs. In Conv.BF, 30% of total *ΔP* occurs in the cohesive zone and 50% in the lower* furnace (including 2/3 of cohesive zone). For SimpLE BFs, the lumpy zone volume

is increased by 15% (due to thinner cohesive/dripping zones). The results show that the total pressure drop of SimpLE BFs reduces to **43–60%** compared to Conv.BF. The variations in SimpLE BFs are derived primarily from the differences in top gas volume (Table 3).

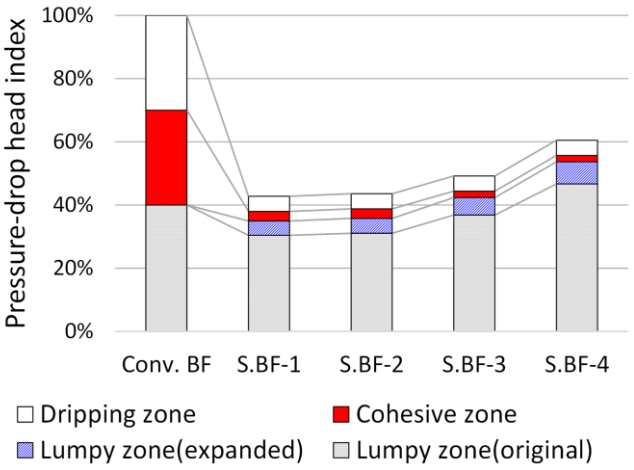

Figure 16. Pressure-drop heads of SimpLE BFs

Considerations: Notably, the resistance in the lower furnace (including the cohesive zone) is reduced to **1/7** of the conventional level. Consequently, the dominant resistance shifts to the lumpy zone. This characteristic implies that gas distribution is governed primarily by stock-line profile control (Smart Charging) rather than complex, hard-to-control lower-furnace phenomena. Furthermore, since Fig. 16 compares pressure-drop *head*, the *actual* pressure drop is likely an additional 20–30% lower in SimpLE BFs due to lower gas density by CR reduction.

5. Discussion

5.1 Synergistic Mechanism for Near-Complete PC Combustion

Limitations of the Filtering Mechanism: While the coke-slit-less cohesive zone functions as an in-furnace filter (Section 4.2), relying solely on this "third mechanism" is insufficient for ultra-low CR operation because the capacity to consume unburnt PC via carburization is inherently limited. Under standard conditions (hot-metal [C] = 4.5%, hearth carburization ratio = 10–20%, and reaction rate ratio $RR_3 \approx 0.5$), the maximum capacity for unburnt PC consumption via carburization is estimated to be only 20–23 kgC/thm.

Necessity of Smart Combustion: If the primary combustion efficiency (primary-η_{pc}) remains at conventional levels, the amount of unburnt PC generated would far exceed this consumption capacity, leading to accumulation in the lower furnace or emission from the top. Therefore, Smart Combustion is not optional but essential to suppress unburnt PC generation to a level that falls within the consumption limit of the "third mechanism".

Conclusion on Integration: SimpLE thus integrates Smart Combustion (minimizing unburnt PC) and Smart Charging (consuming residual PC) to enable near-zero unburnt PC operation.

5.2 Additional CO_2 Reduction and Future Prospects

In the preceding sections, the technical feasibility of ultra-low CR BF was examined in detail. Based on these findings, this section discusses the additional CO_2 reduction potential and explores future prospects for achieving carbon-neutrality (CN).

Surplus Gas Substitution: In Fig. 11, Input C includes carbon derived from fuels used for gas reforming or combustion, such as natural gas. Converting one of a few BFs to an ultra-low CR allows surplus gas from remaining furnaces to replace natural gas. This substitution alone can reduce Input C by an additional 10%.

Metallic Burden Integration: Similarly, if 44% (as Fe) of the burden materials are replaced with metallic feedstocks such as scrap or direct reduced iron (DRI), the reliance on natural gas can be eliminated. This approach yields CO_2 reduction benefits comparable to those achieved through surplus gas utilization.

BOF Gas Recovery: In addition, separate from the measures above, BOF (Basic oxygen converter) gas—which contains relatively low nitrogen—can be treated by oxygen combustion with flue gas recirculation to increase CO_2 concentration. This enables an energy-efficient and facility-compact method to capture an additional 5% of CO_2. Consequently, the total CO_2 reduction illustrated in Fig. 11 can reach as high as 80%.

Pathway to Carbon Neutrality: Furthermore, replacing coal with alternative fuels such as e-fuels, biomass (including waste-derived sources such as MSW), or using plasma heaters may help achieve a fully carbon-neutral or even negative-emission ironmaking process. As noted in Section 1, a novel scheme to utilize municipal solid waste (MSW) as metallurgical reductants is proposed as Step 2 of the SimpLE process [7], reinforcing the long-term potential of the SimpLE process as a sustainable ironmaking solution.

Comparative Advantage vs. Hydrogen-Based Routes: While hydrogen-based DRI (H_2-DRI) combined with an electric melter is often cited as a deep-decarbonization route, it

faces significant challenges in energy efficiency. As indicated in our related study [7], H_2-DRI processes generally require substantially higher gross energy input (more than 3 times that of conventional BFs) due to the energy intensity of hydrogen production. In contrast, SimpLE BF maintains gross energy consumption comparable to conventional BFs while achieving deep Input C reduction through process efficiency and internal gas recycling. This suggests that SimpLE BF offers a more energy-rational and more economical transition pathway, particularly in regions where green hydrogen supply is constrained or costly.

5.3 Technology readiness and Industrial-scale verification

Technology readiness: Fundamentally, the technology readiness level is inherently high because the thermodynamic complexity of the conventional BF—often viewed as a "black-box-like 3-dimensional" mixed-reduction process—is resolved and transformed into a "quasi-one-dimensional" gas-based reduction process consistent with the sophisticated thermodynamic analysis models used for this study. Further, the individual key technologies are already mature or verified: *almost-fully gas-based reduction* [4, 27], *raceway-free PC combustion* [40] , and *coke-slit-less cohesive zone* [44]. Accordingly, while an industrial trial at CR ≈ 60 kg/thm has not yet been conducted, the convergence of the proposed model-based analysis with available industrial datasets within the stated ranges provides sufficient technical justification.

Industrial Feasibility and Verification Strategy: While the feasibility of the theoretical limit (CR ≈ 57 kg/thm) is considered high, concerns may inherently arise simply because it remains an uncharted territory. A significant strength of SimpLE, however, is that it is not constrained to this single operating point (Cases S.BF-1 and -2); rather, it offers the flexibility to continuously select any intermediate value up to CR = 167 kg/thm (Cases S.BF-3 and -4). Within this spectrum, operations comparable to cupolas (CR ≈ 80 kg/thm) [53] and scrap melting furnaces (CR ≈ 140 kg/thm) [44] have already been industrially verified. Therefore, the practical verification challenge is determining how closely industrial operations can approach the 57 kg/thm target. We consider this fully attainable through

engineering optimization, utilizing the conservative analysis margins identified in this study (e.g., conservative parameter settings compared to experimental potentials) if needed.

6. Conclusions

(1) Process Validation and Novelty

This study validates the process-level feasibility of the SimpLE BF (CR ≈ 60 kg/thm), redefining the blast furnace from a "reduction-gasification reactor" to a "high-efficiency melter coupled with a full-gas-based reduction shaft." This paradigm shift is achieved by integrating three operational concepts:

- **Smart Reduction** (temperature-controlled, 100% gas-based reduction via three-stage tuyeres)
- **Smart Combustion** (raceway-free, mild-blast operation; higher primary PC combustion efficiency)
- **Smart Charging** (full-mixed burden with particle-size layering; coke-slit-less cohesive layer)

Smart Reduction thermodynamically transforms a “black-box-like 3-dimensional” mixed-reduction process into a “quasi-one-dimensional” gas-based reduction process, enabling the deductive manipulation of critical variables such as reduction temperature and shaft efficiency. Smart Combustion and Smart Charging serve as indispensable enablers that synergistically support this transformation.

(2) Practical takeaways on permeability

Contrary to prior conventional concerns regarding ultra-low CR, the synergistic effects of the three concepts are estimated to reduce the pressure-drop head in the cohesive-zone to ~1/10 of the conventional value. Consequently, total furnace pressure-drop head decreases to ~43–60%, shifting gas-distribution control from the cohesive zone to the lumpy zone, where permeability is controllable via stock-line profile control (Smart Charging).

(3) System-level implications and Competitiveness

Relative to conventional BFs, SimpLE BF offers significant advantages:

- **Decarbonization:** Input carbon is reduced by ~38–41% (fossil-based) and up to ~53%

(green-H_2). With CO_2 capture, total emission reduction reaches ~60–68%.

- **Energy Efficiency:** Net heat consumption for the entire ironmaking process remains comparable to or lower than conventional BFs.
- **Resource Priority:** Considering energy-system constraints—gross energy demand, availability and economics, the practical priority of fuels for reducing input carbon is identified as: "recycling surplus gas" > CH_4 > H_2.
- **Advantage over Hydrogen-based Routes:** Unlike hydrogen-based routes (e.g., such H_2-DRI+Melter), which requires over 3 times the gross energy for conventional BFs and rely heavily on green hydrogen infrastructure, SimpLE offers a robust pathway achievable with significantly lower energy penalty. It enables deep decarbonization even in regions where green hydrogen supply is constrained or costly.

(4) Technology readiness

While an industrial trial at CR ≈ 60 kg/thm is yet to be conducted, the technical feasibility is supported by both the robustness of the “quasi-one-dimensional” gas-based reduction process and the maturity of the individual constituent technologies—namely, gas-based reduction, raceway-free combustion, and coke-slit-less cohesive zones—separately verified in industrial environments. With intermediate operations (CR ≈ 80 kg/thm) proven in cupolas, the logical next step will be an industrial-scale verification to bridge the gap toward the theoretical limit (CR = 57 kg/thm).

(5) Future Outlook

Future work will focus on plant-level engineering, including geometric design and scale-up, and exploring the integration of circular carbon resources such as MSW to achieve carbon neutral and even negative emissions.

Data Availability Statement

The data that support the findings of this study are available from the corresponding author, [Takeshi Sekiguchi], upon reasonable request. A significant portion of the data is also available within the cited literature in the reference list.

Acknowledgements

The author gratefully acknowledges Mr. Tsutomu Fukushima and Mr. Katsuaki Iwasaki, his respected former colleagues at Nippon Kokan K.K., for their valuable comments and insightful advice on this manuscript.

Conflict of Interest Statement

The author declares that he has no conflict of interest.

Nomenclature --- See Appendix A for expanded nomenclature

CKD	Coke dust
CR	Coke rate (*kg/thm*)
De-CO_2	CO_2 separation/treatment facility
D_p	Particle diameter (*m*)
DRR	Direct reduction ratio (%)
Input C	Input carbon (*kgC/thm*)
K	Permeability resistance coefficient
OD	Oxidation degree, OD ≡ (CO_2 + H_2O)/(CO + CO_2 + H_2 + H_2O)
P	Gas absolute pressure (*MPa*)
ΔP	Pressure drop (*MPa*)
PC	Pulverized coal (or char)
PCR	PC rate (*kg/thm*)
primary-η_{pc}	η_{pc} by the oxygen from PC or tuyere blast (÷)
Q	Heat transfer rate (*kJ/s*)
RD	Reduction degree (of iron ore; %)
RR	Reaction rate ratio of PC to Coke (R_{pc}/R_{ck})
T	Gas temperature (*K*)
TGR	Top Gas Recycle
t	Cohesive zone average thickness (*m)*
u, u_0	Gas actual velocity / superficial velocity (*m/s*)
UPC	Unburnt PC
V_g	Gas flow rate (m^3/s)
X, X_G	PC-to-oxygen ratio and its gasification limit ($kgPC/Nm^3O_2$)
x, y	Molar ratio of PC/Coke(C) to oxygen(O) (*molC/molO*)

Greek characters

ε	Void fraction (÷)
η_{pc}	PC combustion efficiency (÷); Carbon-based standard

References.

[1] Ariyama T. "Perspectives on the promising pathways to zero carbon emissions in the steel industry toward 2050". *ISIJ Int* 2025;65:165–184. doi:10.2355/isijinternational.ISIJINT-2024-320

[2] Ariyama T. "Perspective toward long-term global goal for carbon dioxide mitigation in steel industry". *Tetsu-to-Hagané* 2019;105:567–586. doi:10.2355/tetsutohagane.TETSU-2019-008 (in Japanese).

[3] Naito M. "Development of ironmaking technology". *Nippon Steel Tech Rep* 2006;94:2–15. Available from: https://www.nipponsteel.com/en/tech/report/nsc/pdf/n9402.pdf [accessed 2025-09-27].

[4] "ULCOS top gas recycling blast furnace process (ULCOS TGRBF). Final report". *EUR 26414 EN*. Brussels: European Commission, Research Fund for Coal and Steel; 2014. doi:10.2777/59481

[5] "New blast furnace process (ULCOS). Final report". *EUR 25085 EN*. Brussels: European Commission, Research Fund for Coal and Steel; 2013. doi:10.2777/28645

[6] Nakano K, Sakai H, Ujisawa Y, et al. "Development of low carbon blast furnace operation technology by using experimental blast furnace". *ISIJ Int* 2022;62:2424–2432. doi:10.2355/isijinternational.ISIJINT-2022-117

[7] Sekiguchi T. "Beyond Carbon Neutral with Ultra-low Coke-rate Blast Furnace (#226)". In: *European Steel Technology and Application Days (ESTAD 2025)*; 6–9 Oct 2025; Verona, Italy. Forthcoming.

[8] Ito R, Yoshida Y, Hoshino K, et al. "Blast furnace high pulverized coal rate injection at Kobe Steel". *Kobe Steel Eng Rep* 2000;50(3):6–11. (in Japanese).

[9] Yatsuzuka T, Nkayama K, Omori K, et al. "Injection of Reducing Gas into Blast Furnace (FTG Process)". *Transactions of ISIJ* 1973;13:115–124. doi:10.2355/isijinternational1966.13.115

[10] Ariyama T, Sato M, Sato T, et al. "Desirable coke properties for blast furnace in future". *Tetsu-to-Hagané* 2006;92:114–121. doi:10.2355/tetsutohagane1955.92.3_114 (in Japanese).

[11] Iwanaga Y. "Investigation on behavior of unburnt pulverized coal in blast furnace". *Tetsu-to-Hagané* 1991;77:71–78. doi:10.2355/tetsutohagane1955.77.1_71 (in Japanese).

[12] Yamaguchi K, Ueno H, Tamura K. "Maximum injection rate of pulverized coal into blast furnace with consideration of unburnt char". *Tetsu-to-Hagané* 1992;78:1214–1221. doi:10.2355/tetsutohagane1955.78.7_1214 (in Japanese).

[13] Tamura K, Ueno H, Yamaguchi K, et al. "Upper limits to combustibility of pulverized coal in blast furnace raceway and desirable injection position". *Tetsu-to-Hagané* 1991;77:775–782. doi:10.2355/tetsutohagane1955.77.6_775 (in Japanese).

[14] Ohno Y, Furukawa T, Matsuura M. "Combustion behavior of pulverized coal in a raceway cavity of blast furnace and a large amount injection technology". *Tetsu-to-Hagané* 1992;78:50–57. doi:10.2355/tetsutohagane1955.78.1_50 (in Japanese).

[15] Hatano M, Miyazaki T, Yamaoka H, et al. "Development of a new ironmaking process using pulverized coal as main fuel and oxygen injection". *Sumitomo Search* 1985;31(3):3–12. (in Japanese).

[16] Nakamura M, Sugiyama T, Ueno T, et al. "Configuration of the raceway in the experimental furnace". *Tetsu-to-Hagané* 1977;63:28–36. doi:10.2355/tetsutohagane1955.63.1_28 (in Japanese).

[17] Ariyama T, Sato M, Murai R, et al. "Combustion behavior and gas flow change in raceway at massive coal injection in experimental furnace". *Tetsu-to-Hagané* 1995;81:1114–1119. doi:10.2355/tetsutohagane1955.81.12_1114 (in Japanese).

[18] Yamagata C, Suyama S, Horisaka S, et al. "A fundamental study on the internal state of the blast furnace at high pulverized coal injection". *Sumitomo Metal* 1992;44(1):36–44. (in Japanese).

[19] Kondo S, Nakamura M, Sugiyama T, et al. " [Effect of coke properties on raceways] ". *Tetsu-to-Hagané* 1975;61:A5–A8. (in Japanese).

[20] Yamaoka H, Nakano K. "Mechanism of the degradation of coke size in raceway". *Tetsu-to-Hagané* 2000;86:733–740. doi:10.2355/tetsutohagane1955.86.11_733 (in Japanese).

[21] Watakabe S, Murao A, Goto S. "Application of high-ratio coke mixed charging technique to the blast furnace". *JFE Tech Rep* 2008;22:49–54. Available from: https://www.jfe-steel.co.jp/research/giho/022/pdf/022-11-2.pdf [accessed 2025-09-27]. (in Japanese).

[22] Hotta H, Yanaka H, Yamamoto R, et al. "High temperature properties of mixed layers of iron ore and coke". *Tetsu-to-Hagané* 1984;70:S814–S814. doi:10.2355/tetsutohagane1955.70.12_S773 (in Japanese).

[23] Ono K, Hida Y, Shigemi A, et al. "The shrinkage of burden materials and pressure drop of gas in softening and fusing zones of blast furnace". *Tetsu-to-Hagané* 1975;61:777–786. doi:10.2355/tetsutohagane1955.61.6_777 (in Japanese).

[24] Ueda S, Miki T, Murakami T, et al. "Agenda for low reducing agent operation of blast furnace". *Tetsu-to-Hagané* 2013;99:1–11. doi:10.2355/tetsutohagane.99.1 (in Japanese).

[25] Kawashiri Y, Nouchi T, Matsuno H. "Effect of nitrogen-less reducing atmosphere on permeability of cohesive layer in blast furnace". *Tetsu-to-Hagané* 2018;104:467–471. doi:10.2355/tetsutohagane.TETSU-2018-022 (in Japanese).

[26] Watakabe S, Miyagawa K, Matsuzaki S, et al. "Operation trial of hydrogenous gas injection of COURSE50 project at an experimental blast furnace". *ISIJ Int* 2013;53:2065–2071. doi:10.2355/isijinternational.53.2065

[27] Hamadeh H, Mirgaux O, Patisson F. "Detailed modeling of the direct reduction of iron ore in a shaft furnace". *Materials* 2018;11:1865. doi:10.3390/ma11101865

[28] Ishimitu A, Sigemi A, Higasi T. "The reduction of iron ore by N2+CO+H2". *Tetsu-to-Hagané* 1959;45:893–895. doi:10.2355/tetsutohagane1955.45.9_892 (in Japanese).

[29] Kodama K, Sigemi A, Higasi T. "Effect of reducing temperature and reducing gas content on reduction of iron ore". *Tetsu-to-Hagané* 1960;46:1138–1139. doi:10.2355/tetsutohagane1955.46.10_1138 (in Japanese).

[30] Usui T, Ohmi M, Hirashima S, et al. "Kinetic analysis on the rate of stepwise reduction of a single sinter with CO–CO2–N2 gas mixture". *Tetsu-to-Hagané* 1987;73:1956–1963. doi:10.2355/tetsutohagane1955.73.15_1956 (in Japanese).

[31] Kamijo T, Iwakiri H, Kiguchi J, et al. "Estimation of coke degradation in the blast furnace considering the strength distribution in the lumpy coke by solution loss reaction". *Tetsu-to-Hagané* 1987;73:2012–2019. doi:10.2355/tetsutohagane1955.73.15_2012 (in Japanese).

[32] Renewable Energy Institute. "The path to green steel—pursuing zero-carbon steelmaking in Japan". 2023. Available from: https://www.renewable-ei.org/pdfdownload/activities/REI_greensteelEN2023.pdf [accessed 2025-09-27].

[33] Japan Institute of Energy, editor. *Sekitan-no kouon-gasuka to gasukahatsuden gijutsu* [*High-temperature coal gasification and gasification power generation technology*]. Tokyo: IPC; 1994. p.88. (in Japanese).

[34] Szekely F, Evans JW, Sohn HY. *Gas–solid reactions*. New York: Academic Press; 1976. ISBN 978-0-12-680850-6. doi:10.1016/B978-0-12-680850-6.X5001-X

[35] Sato M, Murai R, Ariyama T. "Development of one-dimensional mathematical model for pulverized coal combustion considering particle dispersion". *Tetsu-to-Hagané* 1996;82:731–736. doi:10.2355/tetsutohagane1955.82.9_731 (in Japanese).

[36] Nogami H, Ueki Y, Murakami T, et al. "Aspects from powder behavior to ensure burden bed permeability for low carbon operation of blast furnace". *Tetsu-to-Hagané* 2014;100:227–245. doi:10.2355/tetsutohagane.100.227 (in Japanese).

[37] Yamaoka H, Kamei Y. "Experimental study on an oxygen blast furnace process using a blast furnace test plant". *Tetsu-to-Hagané* 1991;77:2099–2106. doi:10.2355/tetsutohagane1955.77.12_2099 (in Japanese).

[38] Sato M, Murai R, Ariyama T, et al. "Development of injection lance with high combustibility for high rate coal injection". *Tetsu-to-Hagané* 1998;84:37–42. doi:10.2355/tetsutohagane1955.84.1_37 (in Japanese).

[39] Kunitomo K, Orimoto T, Nishimura T, et al. "Effects of volatile matter of pulverized coal on reducing agents rate of blast furnace and combustion behavior of coal mixture". *Tetsu-to-Hagané* 2004;90:190–197. doi:10.2355/tetsutohagane1955.90.4_190 (in Japanese).

[40] Shibaike H, Takamiya K, Naito M. "Gasification and combustion behavior of combustibles injected into coke bed". *Tetsu-to-Hagané* 2003;89:1093–1098. doi:10.2355/tetsutohagane1955.89.11_1093 (in Japanese).

[41] Levenspiel O. *Chemical reaction engineering*. 3rd ed. New York: Wiley; 1999. ISBN 978-0471254249.

[42] Hinze J.O. *Turbulence*. 2nd ed. New York: McGraw-Hill; 1975. ISBN 978-0070290372.

[43] Inaba S, Yagi J. "Outlook of pulverized coal injection into a blast furnace". *Tetsu-to-Hagané* 1992;78:1187–1197. doi:10.2355/tetsutohagane1955.78.7_1187 (in Japanese).

[44] Kamei Y, Miyazaki T, Yamaoka H. "Scrap melting using a shaft furnace with coke packed bed injected with highly oxygen enriched air and a large quantity of pulverized coal". *ISIJ Int* 1993;33:267–274. doi:10.2355/isijinternational.33.267

[45] Sugiyama T. "Experimental and numerical analysis on the movement and the accumulation of powder in the deadman and the dripping zone of blast furnace". *Tetsu-to-Hagané* 1996;82:29–34. doi:10.2355/tetsutohagane1955.82.1_29 (in Japanese).

[46] Ichida M, Nakayama T, Tamura K, et al. "Movement and accumulation of fines generated in the blast furnace". *Tetsu-to-Hagané* 1992;78:1132–1139. doi:10.2355/tetsutohagane1955.78.7_1132 (in Japanese).

[47] Narita K, Sato T, Maekawa M, et al. "Report on dissection of Amagasaki No. 1 blast furnace". *Tetsu-to-Hagané* 1980;66:1975–1984. doi:10.2355/tetsutohagane1955.66.13_1975 (in Japanese).

[48] Shimizu H, Sato K, Kojima M, et al. "Investigation of coke degradation behavior in blast furnace". *Tetsu-to-Hagané* 1986;72:195–202. doi:10.2355/tetsutohagane1955.72.2_195 (in Japanese).

[49] Shigemi A. *Seisen [ironmaking] handbook*. 1st ed. Tokyo: Chijinshokan; 1979. p.183. (in Japanese).

[50] Fukutake T, Okabe K. "An influence of high top-pressure operation on pressure drop in a blast furnace". *Tetsu-to-Hagané* 1971;57:1627–1635. doi:10.2355/tetsutohagane1955.57.10_1627 (in Japanese).

[51] Fukutake T, Okabe K. "Empirical formulae for the gas pressure drop and the liquid holdup for the counter-current region of gas-liquid flow in the dropping zone of a blast furnace". *Tetsu-to-Hagané* 1980;66:1947–1955. doi:10.2355/tetsutohagane1955.66.13_1947 (in Japanese).

[52] Ikegami H. "Recent progress and future prospects in blast furnace fuel injection". *Tetsu-to-Hagané* 1972;58:559–565. doi:10.2355/tetsutohagane1955.58.5_559 (in Japanese).

[53] ASM International. ASM Handbook, Volume 15: Casting. Materials Park, OH: ASM International; 2008.